NASA-CR-197907

NASA GRANT FINAL REPORT

SUPPORTED TRANSITION METAL CATALYSTS FOR *PARA*- TO *ORTHO*-HYDROGEN CONVERSION

Christopher J. Brooks, Wei Wang and Darrell P. Eyman

University of Iowa
Department of Chemistry
Iowa City, Iowa 52242

May 1994

Prepared for
Lewis Research Center
Under Grant NAG 3-893

TABLE OF CONTENTS

LIST OF TABLES

LIST OF FIGURES

I. INTRODUCTION

A. Ortho–and *Para*–Hydrogen Theory

Molecular hydrogen can exist in two distinct forms; *ortho*–H_2 and *para*–H_2. The difference between these two forms is that they possess different nuclear spins. *Ortho*–H_2 has the nuclear spins of the two hydrogen atom protons aligned in the same direction, or spin unpaired. This results in total spin having values of +1, 0, and −1. However, for *para*–H_2, the nuclear spins of the two protons are in the opposite direction, or spin paired,[1] and the total spin equals zero.

The composition of the two forms of hydrogen is dependent upon temperature. At high temperature, > −50 °C, the composition is approximately 75% *ortho*–H_2 and 25% *para*–H_2. At high temperatures, the distribution is determined by the spin degeneracy and can be calculated by the formula 2S +1. For *ortho*–H_2, (S = 1), there is a three–fold degeneracy, while *para*–H_2 (S = 0) has only a one–fold degeneracy. This degeneracy is portrayed in Figure 1, with α indicating spin = 1/2 and β indicating spin = −1/2. There are three degenerate forms of *ortho*–H_2 which lead to a total spin of one, while there is only one degenerate form of *para*–H_2 with a total spin of zero. This three to one ratio leads to the composition which is referred to as normal hydrogen. However, if hydrogen gas at room temperature is cooled to the normal boiling point of hydrogen, there is a conversion of the *ortho*–H_2 to *para*–H_2 as the temperature is decreased. In fact, the equilibrium composition of liquid hydrogen is made up almost entirely of the *para*–H_2 form (99.79%). The equilibrium composition of hydrogen between the two above described extremes is a function of

temperature. This is shown in Figure 2.[1,2] This total distribution can be calculated by the summation of the partition function of the nuclear spin rotational energy levels as shown in the equation below. Summation of all even J values refers to distribution of *para*–H_2, while the summation of the odd J values refers to the distribution of *ortho*–H_2.[3]

$$z_{nsr} = \Sigma_{even\ J}\ (2J + 1)e^{-J(J+1)85.3/T} + 3\ \Sigma_{odd\ J}\ (2J + 1)e^{-J(J+1)85.3/T}$$

The range of this catalytic study was from approximately −125°C to the liquid nitrogen temperature composition of 50% *ortho*– 50% *para*–H_2 at −196 °C. This range is displayed in the box in Figure 2.

Although the conversion of *ortho*– to *para*–H_2 is a thermodynamically favored process, it is also a very slow one. In fact, if normal hydrogen is liquefied, the resulting liquid has practically the room temperature composition. Over time, this mixture will convert to the thermodynamically favored product, *para*–H_2. Therefore, to interconvert between the two forms of hydrogen with any appreciable rate, a catalyst must be employed.

The question may be asked why there is a need to study the catalytic conversion of *ortho*– to *para*–H_2. To answer this, one must first understand a little more about the reactions involved. The conversion of *ortho*– to *para*–H_2 is exothermic. In fact, the heat of conversion (0.338 kcal/mol) is over 1.5 times greater than the latent heat of vaporization (0.213 kcal/mol).[1] As stated before, following the liquefaction of hydrogen, the liquid hydrogen would have a composition of nearly 75% *ortho*–H_2. Since the heat of conversion is greater than the heat of vaporization, there would be considerable loss of H_2 due to boil–off

as the *ortho*–H_2 slowly converts to *para*–H_2 in the storage vessel. This occurrence can be reduced if a catalyst is used to convert the *ortho*– to *para*–H_2 while cooling in the gas phase. This will help to dissipate the heat of conversion before the *ortho*–H_2 converts to *para*–H_2 in the liquid phase.

Liquid H_2, which is almost entirely *para*–H_2 at equilibrium, is considered by many as fuel for hypersonic flight, mainly because of its high energy density. Since the conversion of *ortho*–H_2 to *para*–H_2 is reversible, the corresponding reverse reaction, *para*– to *ortho*–H_2 is endothermic. This endothermic reaction can provide a heat sink, which can be utilized to cool the various parts of the aircraft. However, this endothermic conversion proceeds far too slowly for practical use. The use of a catalyst speeds up the rate of this endothermic reaction. Therefore, it is a combination of both the slow inherent rate of the reaction along with the high heat of conversion that make the interconversion of *ortho*– and *para*– H_2 an interesting process to study.

B. Theory of *Ortho*– and *Para*– Hydrogen Catalysis

It was reported in 1933 by Farkus and Sachsse that *para*–hydrogen was converted rapidly at room temperature to normal hydrogen (75 % *ortho*–H_2 and 25 % *para*–H_2) in the presence of paramagnetic molecules in the gas phase or paramagnetic ions in solution. The conversion was also reported to be second order in nature.[4] In that same year, Wigner derived an equation to explain the relationship between the rate of *ortho*– and *para*–H_2 interconversion and the magnetic moments of paramagnetic species and the magnetic moment of the proton, along with the distance from the paramagnetic center to the proton.[5] This relationship is shown in the following equation:

$$\text{Rate} \propto \frac{\mu^2(M)\ \ \mu^2(H_2)}{r^8}$$

where μ (M) and μ (H_2) are the magnetic moments for the paramagnetic species and the proton, respectively. The distance between the paramagnetic center and the hydrogen is defined by r.

A further analysis was done in 1973 by Petzinger and Scalapino[6] and more recently by Coffman.[7] Their studies once again derived the equations which explain the rate in which *ortho*– and *para*–H_2 interconvert. The results were very similar to the initial study by Wigner. It was concluded that the rate was proportional to the magnetic moments of the hydrogen and the paramagnetic center divided by the distance of the hydrogen to the paramagnetic center. However, the distance was to the sixth power as opposed to distance being to the eighth power as proposed by Wigner. This relationship is presented in the following equation:

$$\text{Rate} \propto \frac{\mu^2(M)\ \ \mu^2(H_2)}{r^6}$$

This equation is of importance in understanding the studies reported here. It helps to describe ways in which the properties of a catalyst can be altered in the hopes of improving the rate of *ortho*– to *para*–H_2 catalysis. It states that increasing the magnetic moment of the

catalyst active metal will increase the rate exponentially. Also, and more importantly, by decreasing the distance between the reactant H_2 and the surface, an increase in activity should be seen that grows exponentially by a power of six. These are the two areas in which the efforts were directed during the synthesizing of catalysts.

Another theory was presented in 1983 by Stevenson on the mechanism of *ortho*– and *para*–H_2 interconversion by diamagnetic substances.[8] It was stated that any local magnetic or electrical field would enhance *ortho*– to *para*–H_2 conversion. Work by Van Cauwelaert and Hall support this theory as they studied the conversion of *para*–H_2 over alumina.[9] Their study completely eliminated the possibility of the reaction being caused by paramagnetic centers. They felt the magnetic moment of the exposed ^{27}Al nuclei was partially responsible for the conversion. The authors also noted that the addition of transition metals with paramagnetic properties will cause more intense magnetic centers and increased rates.

It was stated earlier by Farkus that the conversion of *para*–H_2 to normal H_2 by gas or solution phase paramagnetic species at room temperature was second–order in nature. It has been further shown that the order of the reaction is dependent upon the reaction conditions. In the absence of a catalyst, the *ortho*– to *para*–H_2 conversion is a second–order reaction.[10] However, in the presence of a catalyst, the reaction approaches first–order for a gas phase reaction.[11] This reaction is the one that is presently under investigation. However, if a catalyst is added to liquid phase hydrogen, the reaction is considered to be zero–order in nature.[10]

C. History of *Ortho*– to *Para*–Hydrogen Catalysts

1. Rare Earth Oxide Catalysts

The history of *ortho*– and *para*–hydrogen catalysts date back to the initial studies by Farkus in 1933. However, the majority of the work to date has been attempts to understand the theory and/or the mechanism of *ortho*– and *para*– hydrogen interconversion as opposed to developing catalysts with high activities which could be scaled up for industrial use.

Selwood did extensive research into the conversion rate of *ortho*– and *para*–hydrogen over the rare earth oxides europia (EuO) and lutetia (Lu_2O_3), and ytterbia (Yb_2O_3) along with the other oxides yttria (Y_2O_3) and chromia (Cr_2O_3). In the case of yttria and lutetia, the rate of reaction was reported to be dependent upon the temperature of pretreatment of the oxide.[12] As the temperature of pretreatment in H_2 gas increased, so did the liberation of water molecules and the activity. This was believed to be caused by reduction of the metal oxide to form a paramagnetic site. This process then liberated the water. In the work with europia and chromia, conversion was determined at temperatures between 65 K and 187 K. It was of interest to determine whether the rate of conversion changes as the temperature of conversion is passed through the Curie temperatures. These are the temperatures where the transition of ferromagnetic EuO or antiferromagnetic α–Cr_2O_3 to the paramagnetic version of both species was expected. What was found was little change in the rates at those temperature.

Further study on *para*–H_2 conversion over neodymium and dysposium oxides was conducted by Eley.[13] Their results were similar to those of Selwood as activity increased with the increased temperature of outgassing. The increase in activity was believed to be caused by loss of oxygen during outgassing. Electron transfer would affect the surface paramagnetic

moments by generating cations with valence less than three.

Selwood also studied the effect of an extrinsic magnetic field on the *para*–H_2 conversion rate on rare earth oxides.[14] His studies concluded that the rate of *para*–H_2 conversion could be increased or decreased by an extrinsic field, and was dependent upon the metal and the corresponding intrinsic paramagnetic field. His conclusions were that one could perturb an intrinsic field with an extrinsic magnetic field.

When comparing the rates of the above mentioned catalysts with those presented in our work, comparisons are difficult as the rate constants for different catalysts were often calculated differently by each researcher. However, an estimate of the differences among some selected catalysts will be made. For the Yb_2O_3 catalyst prepared by Selwood, the best rate constant for this catalyst was reported to be 14.2 μmol s^{-1} m^{-2}. This was calculated for the conversion of *para*–H_2 to *ortho*–H_2 at room temperature. Selwood also tested a Gd_2O_3 catalyst during his study of the effects of an extrinsic magnetic field. He measured a rate constant between 170 and 350 μmol s^{-1} m^{-2} when converting *para*–H_2 to *ortho*–H_2 as above. This activity was without the external magnetic field. However, when calculating a rate constant for CB–II–88, a ruthenium catalyst having excellent activity, the rate constant was estimated to be approximately 106,000 μmol s^{-1} m^{-2}. This value was calculated using a measured activity and the ruthenium surface area using measured active gas adsorption. From this it is easy to see that catalysts prepared in this work have greater activity then catalysts prepared by Selwood.

2. Transition Metal Catalysts

Transition metals were evaluated as catalysts for the interconversion of *ortho*– and

para–hydrogen. In 1975, Rudham reported *para*–hydrogen conversion using catalysts prepared by exchanging low concentrations of Mn, Co, Ni, Cu, Zn, and Pd onto an X–zeolite support.[15] It was observed that the rate increased relative to that of the support itself for all metals studied except Zn. However for Pd, the activity was not as great as that of the other active metals.

In 1968, Singleton and coworkers at Air Products and Chemicals, Inc. completed a study in which they developed a rate model for the *ortho*– and *para*–H_2 interconversion.[16] Their study reported the effects of temperature and concentration gradients within a catalyst particle as well as the effects of other process parameters. This study was done using a highly active catalyst reported to be a nickel silicate supplied by Air Products.

Barrick and coworkers studied the conversion of *ortho*– to *para*– at –196 °C over iron oxide gel catalysts. Their study was to find improvements for both preparation and activation of the catalysts.[17] They reported several results which were of interest for our study. The preparation techniques and the purity of reagents were highly important. Catalytic activity varied due to how rigorously a catalyst was washed following preparation, and how pure the $FeCl_3$ precursor was prior to catalyst preparation. It was also reported that activity was dependent upon the activation conditions. Catalysts had better activities when activated at higher temperatures and for shorter times. Also, it was reported that the purity of reactant hydrogen was important to obtain consistent results.

The most comprehensive study to date was by Haley and Hinden for Englehard Industries in 1965.[18] Their study consisted of testing the Groups VIIIA and IB metals in various forms for *ortho*– to *para*– conversion at –196 °C. They tested a variety of different

catalysts which showed a wide range of activities. When testing a finely divided metal or finely divided metal alloy as a catalyst, it was found that ruthenium or alloys containing ruthenium displayed the best activity. When the Group VIIIA and IB metals were supported on alumina, the ruthenium and nickel supported catalysts were the only ones with at least moderate activity. When the support was changed to activated carbon or silica, ruthenium was again found to be the best metal compared to the others mentioned. It was also found that 10% ruthenium supported on silica was more active than the corresponding 30% ruthenium on silica catalyst.

From the above referenced literature, the metals iron, nickel and ruthenium as well as the lanthanides showed promise as catalysts for *ortho*– to *para*–H_2 conversion. However, any metal which has paramagnetic properties should be considered as a candidate if a catalyst with suitable surface properties can be prepared.

D. Reactor System

The reactor designed to test the conversion of *ortho*– to *para*–H_2 is a standard plug–flow reactor operating under integral conditions.[19] A reactor of similar design is discussed by Haley and Hindin in the Engelhard Technical Report.[17] The following is a discussion of the theory behind *ortho*– and *para*–H_2 detection as well as modifications made to the previously referenced reactor design.

The method of analyzing gas mixtures dependent upon thermal conductivities is a highly developed technique.[20] Since, as shown in Figure 3, the thermal conductivities of *ortho*– and *para*–H_2 differ to about 400 °C, one can take advantage of this using a thermal conductivity detector (TCD).[21] The TCD filaments are aligned to form the four arms of a

Wheatstone bridge. These filaments are divided into two pairs, with each pair having matched resistance. Each filament is in a cavity for separate gas flow. Reference normal H_2 (75% *ortho*, 25% *para*) is passed across one pair at 150 mL/min and the test H_2 is passed at a matched flow rate across the other pair. At a total bridge current of 175 milliamp the bridge imbalance is measured as a millivolt (mV) potential across a 10K Ω resistor. If the test flow is Normal H_2, there is no bridge imbalance. If the test flow contains excess *para*–H_2, one gets a positive mV response. Any other contaminant (N_2, He, H_2O, etc.) will give a negative mV response. Figure 3 also shows that since the thermal conductivity difference decreases with increasing temperature, the measurement should be at the lowest stable temperature allowed by the bridge. Following a 1/2 hour (h) warm–up period in which the bridge is energized, this temperature was determined to be approximately 40 °C. A simplified detector schematic is shown in Figure 4.

The bridge was calibrated quantitatively using the following procedure. Air Products nickel silicate was placed in two separate reactors that were in series with each other. Each reactor contained approximately a ten fold excess of the amount of catalyst needed to convert to the equilibrium composition at –196 °C. At that temperature, the 25% excess of *para*–H_2 in the test stream leads to a bridge imbalance measured as 2.48 mV. Assuming the response is linear, one can conclude that for each percent of excess *para*–H_2, a 0.099 mV response is measured. For example, a measured response of 1.23 mV would lead to the calculation of an *ortho*– and *para*– composition of 62.6% and 37.4%, respectively.

A more detailed reactor schematic is illustrated in Figure 5. It consists of 2 separate reactor tube assemblies which are described in more detail later. These reactor assemblies

can be heated up to 600 °C using column mantles (Glass–Col), or cooled in a Dewar flask of liquid nitrogen or other low temperature slurries for catalytic testing. Temperature is controlled to ±1 °C in the heating cycle by a Type K thermocouple temperature controller (Omega).

All components are constructed of 303 or 316 stainless steel (Valves and tube fittings; Swagelok Co.; Tubing; Alltech Inc.). Pressure gauges are constructed of 316 stainless steel inner components, (Ashcroft) while flowmeters are 130 mm Pyrex glass tubes with stainless steel or glass floats (Cole–Parmer).

For activation of a catalyst, one can chose either He (Air Products High Pressure; 99.995% pure) or H_2 (Air Products UPC grade; 99.999% pure) gases, along with the choice of compressed air or vacuum. During activation, these gases are passed across the catalyst bed at a flow rate of 50–100 mL/min and vented to a hood.

For testing of a catalyst, UPC H_2 was split into two streams. A portion is used as the TCD reference flow as described earlier and the remainder is measured by a mass flow controller (Brooks Instrument Co.) calibrated at 0–30 L/min at 250 psig. Following the mass flow controller, the H_2 is passed across the catalyst bed. The pressure gauges are positioned to allow measurement of the inlet and outlet pressure. These values can be used to calculate a corresponding pressure drop across the catalyst bed. Following the catalyst bed, the total pressure of the catalyzed H_2 was regulated down to 60 psig. This allows easier control of the total flow rate by the two regulating valves. A portion of this test stream (134 mL/min) is matched with the reference flow across the TCD, while the remainder is vented through a flowmeter to the hood. It should be noted that the combined flows of the vent and TCD

should equal the flow rate measured by the mass flow controller.

1. Reactor Tube Evolution

a. Reactor Assembly 1; No Thermocouple

The initial reactor tube assembly can be seen in Figure 6. This reactor assembly consists of a 3 foot length of 1/8" stainless steel tubing which has been wound into a coil with a 4 inch diameter. This serves as a pre–cooler to ensure the H_2 is cooled to the reaction temperature before contact with the catalyst. Following the pre–cooler, the catalyst bed is a 1/4" outer diameter (OD) straight stainless steel tube, 4 inches long. The catalyst was held in place by stainless steel screens (80 mesh; Alltech) between 2 Swagelok unions. Following the second screen, the H_2 flows directly to the detector. This reactor tube assembly is attached to the system through the use of Swagelok Quik–Connects, which allow easy removal and installation of the reactor, without contact with the air.

The reactor tube was later changed from the 1/4" OD tube as described above to a 1/8" OD tube. This dropped the inner diameter from 0.21" to 0.0821" or less than half the original diameter. This was needed for the following reasons. First, with the flow rates obtainable on this reactor, it was necessary to have catalyst samples of 100 mg or less. With this small amount of sample, it was felt that the catalyst bed was too shallow and there was a greater chance that a portion of the H_2 would not come in contact with the catalyst at all. This condition is known as reactant blow–by. With a 1/8" tube, the effective catalyst bed was doubled in length, increasing the chance that every H_2 molecule would come in contact with the catalyst. With the 1/4" tube, activity decreased with increasing flow rates, indicating

blow–by. After changing to the 1/8" tube, the calculated activity remained constant with increasing flow rates, indicating blow–by was eliminated. The second concern was of heat transfer to the center of the tube. Since, as explained earlier, the conversion of *ortho–* to *para–*H_2 is exothermic, there exists the possibility of a temperature gradient developing between the center of the catalyst bed and the outer wall. This could cause the activity measurement made to be at a temperature warmer than the isothermal bath temperature. Reducing the distance between the bed center and the bath should reduce the possibility of a temperature gradient and ensure accuracy in the activity measurements made. An accurate temperature must be known in order to calculate accurate catalytic activity.

b. Reactor Assembly 2; Bent Thermocouple

Reactor Tube Assembly 2 can be seen in Figure 7. The following modifications were made as improvements to the first tube. A VCR fitting (1–3) (Cajon) was placed on a Swagelok tee (4) leading into the catalyst bed. This is to allow easy loading and removal of each catalyst sample. The second improvement was the addition of a thermocouple assembly (7–9) to the base of the catalyst bed. The manifold, a 3/8" OD stainless steel rod with a 1/4" ID internal cavity, was attached to the rest of the assembly by using Swagelok reducers silver soldered into place. The thermocouple itself was a 1/16" OD Type K stainless steel probe (Omega), with the temperature measurement at the tip directly in the gas flow.

The major disadvantage of this assembly was the sharp bend in the thermocouple probe. With the constant removal and insertion of this assembly from a cold dewar or heating mantle, the physical stress on the probe caused electrical shorts to develop in the probe, rendering it useless. Note that contact between the stainless steel manifold and the

probe is several inches from the tip.

c. Reactor Tube Assembly 3; Straight Thermocouple

Further modifications were made to relieve the stress on the thermocouple. These changes are shown in Figure 8. This involved replacing the previous manifold with a larger one, which was 1" in diameter with the same 1/4" internal cavity. The 1/16" OD thermocouple probe was replaced by a 1/8" OD probe with a 1/16" OD reduced tip. This worked much better in terms of physical stability, but the large mass of the manifold and the short distance between the thermocouple tip and the connection point caused a problem. The temperature measured was that of the stainless steel instead of the outlet gas. In fact, the measured temperature on Reactor 3 dropped as much as 30 °C for the same catalyst relative to Reactor 2. Therefore, an accurate temperature measurement could not be made.

d. Reactor Assembly 4; 2 Thermocouples

The final modifications to the reactor tube assembly are shown in Figure 9. To avoid the problems of assembly 3, the manifold was made of 1/2" square stainless steel stock, 6 inches in length with a 1/4" cavity drilled out of the center. This allowed nearly 6 inches between the thermocouple's attachment to the manifold and the tip. To allow added ensurance, a second thermocouple was added at the gas inlet. This was to compare inlet and outlet gas temperatures and ensure that the whole system was at thermal equilibrium. It was concluded through blank cooling and warming runs, as well as the actual testing of a catalyst, that the temperature of peak activity can be measured to ±5 °C.

E. Description of Testing Procedure and Definition of Activity

The following is a discussion of the testing procedure and determination of activity for a catalyst at −196 °C. Approximately 100 mg of catalyst was weighed, placed in a reactor assembly, and inserted into the system. It was then heated for a given time using one of the activation gases as described earlier. The reactor was then cooled in a 2 liter stainless steel Dewar flask filled with liquid N_2. When the vigorous boiling had subsided, the detector response and H_2 flow rate were recorded. The catalyst was removed from the reactor and weighed to determine weight loss due to activation.

Since the present study was not interested in the kinetics of *ortho*– to *para*–H_2 conversion, but rather in developing a highly active catalyst, we were not measuring absolute rate constants, but different catalyst activities were compared using specific reactivity. This value is a measure of how much catalyst is needed to convert a specific amount of H_2 a specific extent at a given temperature. When the specific temperature is −196 °C and the extent of conversion is 70% of maximum, this is defined as β.[17] β can be defined mathematically in the following equation.

$$\beta = \frac{\text{Mass Catalyst} \times \text{Max \% } H_2 \text{ Convertible } (o \text{ to } p) \text{ at -196 °C} \times 70\%}{\text{Mass } H_2 / \text{s} \times \text{\% } H_2 \text{ Converted } (o \text{ to } p)}$$

The mass of the catalyst is measured following reaction, while the mass flow of H_2 is measured by the mass flow controller. This value was kept constant at 22.2 mg/s. The percentage of the hydrogen sample converted from *ortho*– to *para*–H_2 was calculated as described earlier. Since the room temperature composition is 75% *o*-, 25% *p*- and at -196°C

the composition is 50% *o*- and 50% *p*-, the Max % H_2 Converted (*o* to *p*) at −196 °C is 25%. When comparing catalysts, a lower β value indicates a better catalyst, meaning it takes a smaller amount of the catalyst to get the same extent of conversion.

As discussed in the introduction, the kinetics of the catalytic conversion of *ortho*− to *para*−H_2 is first order in nature. It should follow that plotting the −ln[concentration] vs. time, generates a straight line. In this case, a straight line is obtained when plotting −ln[1−conversion] vs. mass catalyst/mass H_2/s. It also follows that a β value can be determined from this plot by finding the value of mg cat/mg H_2 s at −ln[1−70%], which has a value of 1.2. Furthermore, it has been shown that the slope of the line is the sum of the forward (k^1) and reverse (k^{-1}) rate constants.[22] Becaause at equilibrium at −196 °C, the forward and reverse rates are equal, a first order rate constant is equal to 1/2 the slope of the line of this relationship. The values obtained from these two methods are similar with the second method usually giving a slightly higher value. This difference converges as the catalyst improves. From this point on, β^s will indicate a value determined by the first method, while β^m will indicate a value determined by extrapolation of the kinetic plot.

While the intent of this study was to test catalysts at −196 °C, it was discovered that some catalysts show a distinct maximum activity at a temperature warmer than −196 °C. It was shown that while cooling some catalysts to −196 °C, the detector showed a large response before the system reached thermal equilibrium in the liquid N_2. Upon removal of the Dewar flask, the mV response rose as the system warmed. To compare these results, the term β′ was coined. It is similar to β^s with a minor change, as shown in the following equation.

$$\beta' = \frac{\text{Mass Catalyst} \times \text{Max \% } H_2 \text{ Convertible } (o \text{ to } p) \text{ at Temp} \times 70\%}{\text{Mass } H_2 / \text{s} \times \text{ \% } H_2 \text{ Converted } (o \text{ to } p)}$$

Since the measurement is no longer at −196 °C, the possible conversion will decrease with respect to temperature. For example, if the temperature of maximum response is −158 °C, the thermodynamic composition would be 34% *para* and 66% *ortho* leaving the Maximum % of H_2 convertible to be 9% instead of the 25% at −196 °C.

Determination of the temperature of maximum response was done in the following manner. The reactor assembly was cooled to −196 °C. The liquid N_2 Dewar flask was then exchanged for a liquid N_2, 2−methyl butane slurry (m.p. −160 °C), allowing the temperature to rise slowly, at approximately 10 °C per min. When the response reached a maximum, the temperature was recorded. Following determination of that temperature, subsequent trials with the same catalyst were recorded while warming in air instead of the slurry, as the slurry was time consuming and expensive to make repeatedly. The temperatures in air were unreliable due to problems explained in the evolution of the reactor assembly. For those catalysts where the temperature for maximum activity was above −160 °C it was difficult to assign a temperature and the attempts were inconsistent.

II. Metal Silicates

A. Preparation

All catalysts discussed in this section have a specific label which refers to its location in the appropriate table.

1. Iron Silicates

CB–I–1 was prepared using the following general procedure, known as coprecipitation. Into separate burets was placed 15 mL of M $Fe(NO_3)_3$ and 15 mL of 1M Na_2SiO_3. Simultaneously, the solutions were dripped at a rate of 2 drops per second into a stirred solution of 20 mL of 20% w/w $NaNO_3$. This mixture was stirred for 45 min, filtered, and dried at 130 °C overnight.

CB–I–2 used the same coprecipitation procedure except that the $NaNO_3$ solution was replaced with H_2O. Both CB–I–1 and 2 were light gold in color.

2. Chromium Silicates

CB–I–3 was prepared using the following procedure, known as the Sol–Gel method. To a beaker, 100 mL of 1M Na_2SiO_3 was added. To this was added 68 mL of 3M HNO_3, which lowered the pH to 1.7 and caused a gel to form. To this gel was added 100 mL of 1M $Cr(NO_3)_3$ and the mixture was stirred for 1 h. One molar Na_2CO_3 (67 mL) was added to raise the pH to 6.9. This metal gel was suction filtered, washed with H_2O (2 x 100 mL) and MeOH (2 x 100 mL). The catalyst was dried at 23 °C for 2 h followed by 150 °C for 4 h in a vacuum oven.

CB–I–4 was prepared by the coprecipitation method described in the iron silicate section with the following changes. 100 mL of 1M solutions of $Cr(NO_3)_3$ and Na_2SiO_3 were injected into 80 mL of $NaNO_3$. The resulting gel was stirred for 1 h, and was then washed and stirred in MeOH overnight. The catalyst was dried at 110 °C overnight. These catalysts

were light blue in color.

3. Manganese Silicates

CB–I–13 was prepared using the coprecipitation method as described for CB–I–4. Changes include substituting $Mn(NO_3)_2$ for $Cr(NO_3)_3$. All other parameters remained constant. CB–I–29S and 29L were prepared in the same manner as 13 except 29S was aged in the mother liqueur for 5 h, while 29L was aged for 12 h. Both catalysts were treated with MeOH and dried as above. The above gels were initially pink but turned light brown with time, and dried as a light brown solid. CB–I–30 was prepared using the same general procedure, except the synthesis was done anaerobically to prevent the air oxidation of Mn^{2+} to Mn^{3+}. The Mn and SiO_3 solutions were degassed with N_2. The solutions were injected using addition funnels into a three–neck round–bottom flask which was previously evacuated. The gel was kept from air, filtered using a frit, and dried in the vacuum oven at 110 °C. The gel remained pink longer than previous Mn samples, but eventually turned brown. This catalyst preparation was attempted several times to keep the Mn in the +2 oxidation state, but failed.

4. Nickel Silicates

Initial work with nickel silicates involved chemical activation on Air Products HSC 197 Nickel Silicate. A catalyst (AP–DMP) was prepared by refluxing 2 g of AP in 100 mL of 2,2–dimethoxypropane for 2 h. The sample was initially dried at 23 °C, then at 110 °C, all while in a vacuum oven. A similar catalyst (AP–REF) was prepared as AP–DMP except the catalyst was refluxed in MeOH instead of 2,2 DMP. Both of these samples were prepared with the intent of determining the effect of chemical drying on the activity of the catalyst.

CB–I–7 was prepared using coprecipitation as described in CB–I–1 with the following changes. A solution of $Ni(NO_3)_2$ replaced the iron solution. 100 mL volumes of the 1M $Ni(NO_3)_2$ and Na_2SiO_3 were injected into 80 mL of $NaNO_3$; and the catalyst was stirred for 4

h in water, filtered, and dried at 150 °C as above. CB–I–9 and 9M were prepared as above except following filtering, 9M was washed with MeOH overnight, refiltered and dried. CB–I–9MR was prepared by drying and crushing half of 9M, refluxing it in MeOH for 1 h, followed by redrying.

5. Metal/Metal Silicate

The following is a discussion of the impregnation of metal salt solutions on metal silicate supports. Table 1 illustrates the impregnation of $Fe(NO_3)_3$ solutions on Air Products nickel silicate. Approximately 1 g of AP was placed into a 250 mL round–bottom flask and evacuated for 2 h. To this, 5 mL of the iron solution was added *via* a funnel and allowed to sit for the time indicated in the table. The solvent was then removed by vacuum at room temperature and the catalyst was fully dried at 110 °C. The final row in the table, CB–I–22, indicates the substitution of $Cr(NO_3)_3$ for $Fe(NO_3)_3$. Table 2 indicates the impregnation of $Fe(NO_3)_3$ on a previously prepared CB–I–9M silicate. The procedure remained identical to the one described earlier.

B. Catalytic Testing

1. Activity Testing of Air Products Nickel Silicate

a. Activation Time and Temperature

The conditions suggested by the manufacturer for the activation of Air Products catalyst involved heating the catalyst at 150 °C for 4 h under a 20 mL/min He flow. Under these conditions, a β value of 20 was expected, and confirmed experimentally. However, we found that if the catalyst was heated at the same temperature for 12 h instead of 4, the β value increased to 24.0. The catalyst demonstrated deactivation under prolonged heating. On the other hand, it was found that the β value was lowered to 15.7 by heating at 275 °C for

only 2 h. Although this was a commercially prepared catalyst, this result supports the previous claims by Barrick.[23] A distinct color change of the catalyst was noticed as well. Prior to use, the catalyst is bright green in color; it changes to a dull green following activation at 150 °C. The color activation at 275 °C was tan–green, a much duller color than observed at 150 °C. It is felt that the increase in activity can be attributed to the combination of two related factors. First, it is felt that the catalyst becomes more dehydrated by activating at 275 °C vs. 150 °C. This should lower the catalyst weight and make the numerator of the β equation smaller, hence lowering β. This was confirmed by an increase in the percent weight lost during activation at the higher temperature. Second, with the increased dehydration, it should make available more active sites which were occupied by water, also lowering the radius of closest approach for a H_2 molecule to an active site. We feel the various changes in color with respect to the activating temperature give evidence for increased dehydration.

b. Activating Gas or Vacuum

The effect of activating gas was also studied. By activating under H_2 flow at both 150 °C and 300 °C for 2 h, the catalyst lost most activity, giving β values greater than 100. It was believed that the nickel was reduced to Ni^0, as the catalyst turned black in color, was pyrophoric when exposed to the air, and became ferromagnetic. This leads to the belief that Ni^{II} is the active component, rather than nickel metal.

Since it has been shown that activation occurs through dehydration and desorption of the catalyst surface and not reduction, one should be able to activate using a vacuum instead of inert gas flow. By heating Air Products catalyst at 300 °C for 2 h in a vacuum, the catalyst showed a β value of 16.0, which is fairly close to the result achieved with a He flow. The color of the catalyst following vacuum activation was similar to that observed following the He studies. Results of both the time and temperature studies along with the activating gas study are shown in Table 3.

The activity of Air Products catalyst vs. the temperature of conversion is displayed in Figure 10. As shown, there is only modest variation in the β value with respect to the temperature of conversion. The tail for the warmer temperatures is due to inaccuracies for both the measuring of an exact temperature along with the smaller detector response associated with a smaller possible *para*–H_2 conversion. This figure does show that the activity is fairly temperature independent down to −196 °C. This catalyst was tested following He activation for 1 h at 275 °C.

c. Effect of H_2 Flowrate

Initial studies for calibration of the reactor system used Reactor Tube Assembly 1 with a 1/4" OD tube. At low flow rates (less than 5 L/min), β was 27.0 following a 4 h activation at 150 °C in He. As the flow increased, the β decreased to a minimum value of 20.0 at a flow of 15.7 L/min. At higher flows, the β increased with flow until the maximum flow of the reactor was achieved. This can be explained by the following argument. At low flow rates, the pressure drop across a shallow reactor bed is close to zero. With low reactant back pressure, it is felt that the residence time of the reactant on the catalyst surface is lowered, thereby decreasing the possibility of an *ortho*– to *para*–H_2 conversion occurring, increasing β. As the flowrate increases, the back pressure increases accordingly, allowing the H_2 molecule sufficient time on the surface to react, decreasing β. Increasing the flowrate further continued to increase backpressure, but reactant blow–by caused β to increase as well. The H_2 molecules which had time to get to the surface stayed there long enough to react, but some H_2 was blown through the bed without contact with the catalyst.

By switching to a 1/8" OD reactor tube, there was sufficient back pressure at low flowrates. This was caused by the length of the catalyst bed being more than doubled, increasing restriction. The increased bed length also ended the problem of blow–by at the maximum flow of the reactor. By activating Air Products catalyst at 150 °C in He for 4 h, a

β value of 20 was calculated throughout the entire flowrate range of the reactor.

d. Activity of Enhanced Air Products Nickel Silicate Catalyst

Earlier discussion has demonstrated that the activity of AP was increased by an increase in the dehydration of the catalyst. Due to this, an effort was made to chemically remove water. It is known that 2,2–dimethoxypropane should react with water to give methanol and acetone.[24] The resulting organic solvents are much more volatile and easier to remove than water. The β for AP–DMP, the AP sample dehydrated using 2,2–dimethoxypropane, was 16.1 but at the activation conditions of 275 °C in He for only 40 min. In fact, AP–DMP had a β of 40 without activation while unactivated AP showed little activity (β > 100), indicating that the methanol and acetone which replaced water can be partially removed by a room temperature vacuum. AP–M and AP–R were prepared by the washing or refluxing of Air Products catalyst in methanol in the hope for a simple exchange with water. While both gave activities similar to unenhanced AP (β = 16.2; 2 h in He at 275 °C), neither showed activity enhancement. Results of this study are shown in Table 4. Conclusions from this study is that chemical activation helped to shorten the activation time, but did not increase activity.

2. Synthesized Metal Silicates

a. Iron, Manganese, and Chromium Silicates

This is a discussion of the activity of all metal silicates prepared, except nickel. With regard to iron silicates prepared, CB–I–1 had a β of 49.2, while an activity for CB–I–2 was observed to be greater than 100 following activation at 150 °C for 4 h in He. While neither showed exceptional activity, the need for $NaNO_3$ was clearly demonstrated. The Na^+ and NO_3^- ions act as a filler during gel formation, helping to create a porous structure.

The importance of a porous silicate can be seen in CB–I–3 and 4 as well. Both of the

chromium silicates had very low activity ($\beta > 100$) after 150 °C activation. It was felt these catalysts were non-porous, giving a low relative metal surface area for reaction.

More promise was demonstrated with respect to the manganese catalysts. CB–I–13 was nearly as active as AP, with a β of 20.7 (150 °C for 4 h in He). Catalysts CB–I–29S and 29L were never tested, however similar samples prepared by Song[25] and Gloer[26] showed β values between 20 and 40 when activated between 150 °C and 300 °C in He and it was felt there would be no improvement. CB–I–30 was never tested because a silicate with the Mn^{II} oxidation state was never obtained and it was felt the catalytic activity would not differ greatly from other Mn^{III} catalysts. Results from all metal silicates prepared (except Ni) are presented in Table 5.

b. Synthesized Nickel Silicates

With the work done on preparing metal silicates other than nickel, it became obvious that there was difficulty in finding a catalyst with greater activity than Air Products nickel silicate. We therefore shifted our efforts to prepare nickel silicates by various methods. The activities for these synthesized nickel silicates are displayed in Table 6.

CB–I–7 and 9 were prepared using the same procedure and yielded very similar activity (β = 55 and 60, respectively at 150 °C for 4 h in He). However, if the activation temperature was increased to 275 °C, the β value for CB–I–9 dropped to 17.1 It was felt that there was water trapped inside the silicate structure following preparation which was not liberated at 150 °C. By substituting the water used as a solvent in the coprecipitation step for methanol in CB–I–9M, β was lowered to 14.4, even at an activation temperature of 150 °C. Activation at 275 °C lowered β even further to 13.3. We feel this is caused by water having a higher surface binding to the silicate than MeOH. Upon drying, the water clings in the silicate pores, causing them to collapse. MeOH helps to reduce this effect. Also, MeOH is more volatile than water, making it easier to remove.

By refluxing CB–I–9M in MeOH following drying and crushing, CB–I–9MR had a β value of 12.1 following activation at 300 °C. We feel that this can be attributed to catalyst dust trapped in the small pores following crushing. During reflux, air trapped behind these dust particles explodes outward, clearing the pore and increasing the total pore volume. Further evidence of the importance of a large total pore volume was demonstrated by LaBrush.[27] He prepared a nickel silicate (DML–EG) in which ethylene glycol, a larger molecule, was substituted for $NaNO_3$ in solution. This increased the total pore volume, and activity increased to $\beta = 11.0$ following activation at 300 °C.

c. Impregnated Metal Silicates

A study was conducted to determine if the addition of an additional metal to a previously prepared metal silicate would enhance catalytic activity. In this case, the effect of iron impregnation on nickel silicate was studied. As shown in Table 7, the addition of iron to Air Product decreases the catalytic activity. It is felt that this is due to either the loss of equal amounts of more active Ni sites for a less active Fe sites. Similarly, the loss of more Ni sites for less Fe sites, both of equal activity would have the same effect.. The more iron that is added, either by a greater iron concentration of the impregnating solution, or a longer impregnation time, the worse the activity became. However, the addition of iron to CB–I–9M shows a definite increase in catalytic activity, as shown in Table 8. One possible explanation for this is that there are void spaces on the silicate where no nickel was incorporated. Iron would fill those spaces, helping to increase activity. The increase in activity decreases with the amount of iron added. It is felt that the addition of more iron than needed to fill the void spaces would have the same effect as earlier described. In fact, it was further shown by LaBrush[26] that the activity of AP decreased with the addition of Mn^{II} while the activity of a coprecipitated nickel silicate increased with the addition of Ni^{II}.

C. Characterization by N_2 Condensation/Adsorption

Initial characterization of the metal silicates involved measuring total surface area and total pore volume. This was done before catalytic testing could be performed and catalysts were synthesized under the assumption that increased surface area and total pore volume would increase activity. The results presented are for a select group of catalysts, because not all metal silicate catalysts prepared were tested for a total surface area or total pore volume.

Table 9 shows the surface area and pore volume measurements collected during this study. No measurements were collected for iron silicates, as the activity was poor and this class of catalysts was not pursued. Chromium silicates were among the first catalysts prepared. To help determine their quality, surface areas were determined before they were tested for catalytic activity. As one can see, the surface area is only about 1/4 of that of AP. This would agree with the catalytic testing of these catalysts which performed very poorly.

The only manganese catalyst tested was CB–I–13. This catalyst showed a very good pore volume (0.55 cc/g) but an intermediate total surface area (225 m^2/g). It was felt that this catalyst had a larger average pore diameter than AP. Generally speaking, a high population of smaller micropores yields higher total surface areas than a catalyst with the same total pore volume and larger pores. It was hard to conclude anything from these results because the activity of this catalyst was similar to AP.

A more extensive study of nickel silicates was completed. The results obtained were as expected. CB–I–9 had an intermediate surface area and a relatively low pore volume. The activity reflected these trends as it was not as active as AP. However, by washing in MeOH (CB–I–9M) the surface area and pore volume rose dramatically, as did the catalytic activity. This observation would support the previous assumption that a catalyst with a higher surface area and pore volume would be more active. It was proposed that refluxing CB–I–9M in MeOH, would remove small dust particles trapped inside the micropores. The data supports this proposal in that the total surface area increased greatly, while the total pore

volume increased only slightly. This would be expected by decreasing the average pore diameter which would be accomplished by removal of dust from the micropores. DML–EG, a nickel silicate prepared using the MeOH wash technique as well as the substitution of ethylene glycol for sodium nitrate showed an increase in total pore volume as well. This was predicted as ethylene glycol, a larger molecule than sodium nitrate, serves as a larger formation site for the silicate. The surface area for DML–EG was not determined. It was predicted to be less than CB–I–9MR because it should have a larger average pore diameter.

The only impregnated silicate tested was CB–I–12. The surface area was much lower then the original AP. This may be explained by the filling in of a highly complex silicate structure by a metal salt. The complex silicate would have many nooks and crannies which would increase the total surface area. Filling them with the metal salt would lower that surface area. It is unknown whether the number of active sites varies from AP and if they do, by how much.

The main conclusion made from this study was that activity was dependent upon the catalyst having a large total surface area and large total pore volume. With a large total surface area, there is a greater number of metal atoms on the surface. This will yield more active metal sites for catalysis. A large total pore volume helps the mass transport of reactant H_2 through the body of the catalyst particle to the surface. This increases the probability that an H_2 molecule finding the surface will be converted from *ortho*– to *para*–H_2.

First, as displayed with chromium, a very low total surface area generally means poor activity. But as displayed in the nickel catalysts, as the total surface area and pore volume was increased by various modifications in the preparation technique, the activity increased as well. This supports the previous claim that the modifications in preparation (MeOH wash, reflux) did indeed increase pore volume which in turn increased the total surface area of the catalyst, thus increasing catalytic activity.

D. Conclusions for Metal Silicates

When looking at the work done with metal silicates, including enhancing AP, preparing various metal silicates, and impregnating nickel silicates, some conclusions can be made. First, the silicate can only be activated by He, not H_2. This most likely suggests that the activation process is a desorption of water and other adsorbates from the surface, not a reduction of the metal ion to metal. This is further supported by work with AP in which increased activity was observed by increasing the activation temperature. It is felt that the increased activation temperature from the suggested 150 °C to 300 °C reduces the hydration of the catalyst. Water is thought to both increase the catalyst weight and block the distance of a reactant H_2 to the surface, both of which reduce activity.

Second, nickel was the best choice over iron, manganese, and chromium for the preparation of metal silicates. It is unknown whether this is because nickel inherently is a better metal for *ortho*– to *para*–H_2 conversion or if nickel causes the formation of a better metal silicate, which yields a better catalyst surface.

Third, an increase in total pore volume will increase activity. This was displayed with the prepared nickel silicates. Each time an improvement was made to increase the total pore volume, activity increased as well. It is felt that this can be attributed to better mass transport of H_2 through the catalyst. If H_2 has an easier opportunity to get to an active site, it is more likely to be converted. Also, by increasing the pore volume, the total active surface area should increase. Both factors should increase activity. A limit to this effect is most likely the physical stability of the catalyst, as the catalyst become more fragile to crushing.

Finally, additional metal added to a preexisting metal silicate increases activity only if the surface is not already saturated with metal sites. If the surface is saturated, the additional metal will not only add weight, but cover existing sites. Both of these factors will decrease activity.

III. Ruthenium Catalysts

A. Preparation

1. Traditional Ruthenium Catalysts

To a 250 mL round–bottom flask was a weighed amount of pretreated silica support (PQ 1022G; 35–50 mesh) and the mixture was held *in vacuo* for 2 h. To this, the calculated amount of ruthenium salt [$RuCl_3$, $Ru(NO)Cl_3$, or $Ru(NO)(NO_3)_3$] for a desired metal loading was added *via* a separatory funnel. The funnel was then rinsed with 2 mL of H_2O. The resulting mixture was allowed to sit for 5 hours. The solvent was then removed using a rotary evaporator with a bath temperature of 50 °C. The catalyst was dried in a laboratory oven at 130 °C overnight. Ru metal content was determined by weight gain of the support and confirmed spectroscopically. Metal content was determined by spectrophotometric methods described by Beamish.[28] Excess Ru, which had crystallized on the sides of the flask following impregnation and remained following catalyst removal, was washed out and diluted to a concentration of approximately 10 ppm. A 10–mL aliquot of this dilute Ru solution was added to 10 mL of 20% NaCl, 5 mL of 5% $NH_3OH{\cdot}HCl$ and 15 mL of 1,10-Phenanthroline. This solution was adjusted to a pH of 6 with NaOH, diluted to 100 mL, and heated to a boil for 1 h. The absorbance of the resulting yellow solution was measured at 448 nm using a Bauch and Lomb spectrometer. The absorbance was then compared to a standard Ru curve and the Ru metal concentration was extrapolated. Using the dilution factor, the amount of Ru metal remaining in the flask was calculated. $Ru_{(flask)}$ was then subtracted from $Ru_{(init.)}$ to calculate $Ru_{(cat)}$, which was used to calculate a percent metal loading. This method was used for calculation of all traditional ruthenium catalysts preparations.

2. Ruthenium Ammine Precursor Catalysts

Catalysts were prepared by the following general procedure described by Gay[29] and modified by Wu[30]. To a 50 mL beaker, was added a weighed amount of pretreated silica support (PQ 1022G; 35–50 mesh). To this, enough concentrated ammonium hydroxide was added to saturate the support and partially ionize the silanol groups. In a separate 100 mL beaker, the desired amount of ruthenium salt, $Ru(NO)(NO_3)_3$ or $RuCl_3$, was dissolved in 20 mL water, and 2 mL of hydrazine hydrate was added dropwise under constant swirling. When N_2 evolution had slowed, an additional 5 mL of hydrazine was added to ensure completion of the reduction of Ru from 3+ to 2+ and formation of a stable ammine complex. This solution was allowed to sit for 1 hour to permit all N_2 to escape. The Ru^{II} solution and the above mentioned support were mixed and allowed to sit for 16 hours. The catalyst was dried under vacuum for 2 hours and in the air for 16 hours at 115 ° C.

Ruthenium metal content was determined by a spectroscopic determination of K_2RuO_4 concentration as described by Marezenko[31] and Beamish[27]. This involved the oxidation of Ru^0 to Ru^{IV} in a eutectic melt of KNO_3 and KOH at 350 °C.[32] The catalyst was reduced in flowing H_2 at 350 °C overnight in a tube furnace. Approximately 20 mg of the reduced material was weighed and crushed to a fine powder and added to a porcelain crucible. To this was added ≈ 0.5 g of KNO_3 and ≈ 1 g KOH. The mixture was then heated at 350 °C in a muffle furnace overnight. The resulting K_2RuO_4 was dissolved in water, and diluted to 50 mL in a volumetric flask with 2 M NaOH. A sample of the resulting orange solution was centrifuged to remove any remaining silica particulate, and the absorbance of the supernatant was measured at 465 nm using a spectrometer. This value was compared to a standard calibration curve and Ru^{VI} concentration was extrapolated. From this, Ru content of the catalyst was calculated.

3. (η^4–cyclohexa–1,3–diene)(η^6–benzene) Ruthenium (0) Precursor Catalysts

Zinc dust was activated according to Perrin and Armarego[33]. Cyclohexa–1,3–diene was distilled and stored under nitrogen.

Cyclohexa–1,3–diene (4.2 g, 52 mmol) and activated zinc dust were added to a 250 mL round–bottom Schlenk flask. To this was added 8 mL of a $RuCl_3$ (320 mg, 1.23 mmol) solution in ethanol. The resulting blue mixture was stirred at room temperature for 3 h. The final solution, which had turned yellow–brown was purified on alumina, washed with hexane (2 x 30 mL), and the solvent was removed under vacuum. To this yellow solid was added 40 mL of hexane and filtered through a 20 cm alumina column. The resulting solution was reduced to 5 mL and upon cooling to –78 °C, yellow crystals formed. The mother liquor was syringed out and the remaining solvent was dried *in vacuo* to give 0.22 g of (η^4–cyclohexa–1,3–diene)(η^6–benzene) Ruthenium (0) (68 % yield).

The catalyst were prepared using the following general procedure. To a 250 mL round–bottom flask was a weighed amount of pretreated silica support (PQ 1022G; 35–50 mesh) and the mixture was held *in vacuo* for 2 h. To this, the calculated amount of (η^4–cyclohexa–1,3–diene)(η^6–benzene) ruthenium (0) for a desired metal loading was added in 10 mL of anhydrous hexane *via* a cannula. The resulting slurry was allowed to sit overnight and the solvent was removed under vacuum. The catalyst was then stored under nitrogen.

B. Catalytic Testing

1. Activity of Traditional Ruthenium Catalysts

a. Activation Conditions: Time, Temperature, Gas, and Pressure

Results for the catalytic testing of CB–II–20 are shown in Table 10. The number following the result in the text refers to the trial number in the appropriate table. This

catalyst showed little activity at −196 °C, but had good activity at a higher temperature. The temperature of maximum activity was determined using slurry baths to be −158 °C, and this temperature was used to calculate all β' values. Hydrogen was determined to be the best choice for the activation of a ruthenium catalyst. By heating at 335 °C for 4 h in H_2, a β' of 3.8 was calculated (1). This is compared to a value of 6.7 for the same conditions in He (2). However, by increasing the temperature to 450 °C in H_2, the β' dropped to 3.3 (3). Further increase of temperature to 550 °C was counterproductive as β' increased to 3.9 (4). Further increase of the time to 8 h had little effect on activity (12). All of these trials were done with the same activation and reactant gas pressure. From this it was postulated that Ru^0 was the active catalytic species, not Ru^{III}. Increasing the activation gas pressure from 20 to 200 psi had little effect on activity (5,6). The same was true for increasing the reactant H_2 pressure. Activity did not change as the pressure was increased from 200 through 500 psi (1,8–10). Since pressure was not a factor, the value of 200–250 psi was used, with 200 psi being the minimum pressure needed to get the reactant H_2 through the catalyst bed.

The effects of using two gases during activation was also studied. It was postulated that by heating in He prior to reduction, water would be completely removed from the system before reduction. The results of these tests are shown in trials 7 and 11, and seem to have little effect on activity (β'= 3.5 and 3.2, respectfully). However, if one reduces in H_2 at 450 °C, switches to He for 12 h at high temperature, and cools the catalyst to −196 °C in He flow, a β of 8.5 was measured. Exposure of the catalyst at room temperature to H_2 not only increased β, but β' as well. Reheating in He to 450 °C followed by cooling to −196 °C, nearly reestablished the original activity indicating the overall process was somewhat reversible. Reversibility means that following exposure of the activated catalyst to room temperature H_2 the last activity can be regenerated by simply reheating to 450 °C and cooling to −196°C in He as before. This procedure will be referred as "H_2/He activation" the remainder of the report.

CB–II–72 was an 8% Ru/SiO_2 catalyst prepared with the same technique as CB–II–20. The activity test results are shown in Table 11. The results are similar with one exception; the β value following H_2/He activation was greater than CB–II–20 (6). It is unknown why the value went up, although it was important to note that there was an enhancement. It was also discovered that if the catalyst was cooled directly from reduction temperature to −196 °C in flowing H_2 using a liquid N_2 bath, there was some β improvement as well. The rational behind this discovery, known as "Flash Cooling" and the "He Effect" following H_2/He activation, will be discussed in more detail later.

b. Effect of Percent Metal Content

From the previous study, it was determined that the best conditions for activation were to reduce at 450 °C for 4 h in H_2, followed by a 12 h He purge at 450 °C, followed by cooling to −196 °C in He prior to testing. It was shown that the β and β′ measurements displayed only slight variation when the activation temperature ranged from 300 to 500 °C. Therefore, the initial comparison of most catalysts will be reported using β′ while activating at 450 °C, with H_2/He activation results reported as well.

Activities for all $RuCl_3$ precursor catalysts and their varying Ru weight percents are shown in Table 12. CB–II–15, with only 0.1% Ru, showed little activity at any temperature (1-2). But, by adding just 1% Ru, a β′ of 5.0 (4) was achieved. Further increases of Ru gave further increases in activity (6, 8, 10), until the β′ of 3.3 was observed for 8% Ru in CB–II–20 as described above. However in CB–II–46 with 14% Ru, there was a decrease in activity (13).

The use of He as the sole activating gas gave negative results for all catalysts tested (1, 3, 7, 9). However, following H_2 reduction, there was a "He Effect" as before. CB–II–19, with 4.4% Ru, had activity at −196 °C, but was not as active as CB–II–20. The β′ was 36.0, compared to 8.5. Increasing Ru content to greater than 8% had a negative effect on the

"He Effect" β as well. For CB–II–46, β increased to 15.2 (15). Catalysts were also prepared to study the effects of the Ru precursor metal on activity, and an entire range of metal loadings were prepared. However, the majority of this effort was spent testing the ≈ 8% Ru catalysts.

c. Effect of Metal Precursor

Tables 13 and 14 show the activity of a range of Ru catalysts prepared with $Ru(NO)Cl_3$ and $Ru(NO)(NO_3)_3$, respectfully. For the $Ru(NO)Cl_3$ catalysts, β′ activity increased with increasing metal content, but had a definite maximum associated with ruthenium content (1–4). While testing CB–II–24 (9.2% metal loading), it was demonstrated that following reduction, heating in He followed by cooling to −196 °C in He had an effect similar to other catalysts (5). β^s was 13.5 compared to over 75 when reduced and cooled in H_2. Further heating in He had an adverse effect, as β increased slightly (6, 7). Although the majority of activity was regained following exposure to room temperature H_2, it is felt that the activity lost due to repeated heating is due to sintering.

Similar results for β′ are found for the catalysts prepared with $Ru(NO)(NO_3)_3$. The same trend of β′ decreasing with increasing Ru loading followed by a subsequent increase in β′ for high metal loading is evident (1, 3, 7). The main difference is in the −196 °C activity following H_2 /He activation (5, 9). While enhancement is observed, (β = 33.7 for CB–II–27; 30.0 for CB–II–29), it not nearly as great as observed for ruthenium catalysts prepared with chloride containing precursors. Figure 11 illustrates the β′ activity at −158 °C vs. metal content for all Ru catalysts, while Figure 12 illustrates the enhancement activity at −196 °C following H_2 /He activation.

Conclusions that can be made from the study of these ruthenium catalyst are as follows. First, Ru catalysts show low activity at −196 °C following reduction in H_2. Second, Ru catalysts all show activity at temperatures warmer than −196 °C; the temperature of

maximum activity is ≈ −158 °C. Third, the β′ is more dependent upon metal content and less dependent upon metal precursor. Fourth, activity is observed at −196 °C if the catalyst is heated and cooled to −196 °C in He following reduction and prior to exposure to the reactant H_2. Finally, the amount of this enhancement is dependent upon the metal precursor used.

d. Effect of Platinum Metal Addition

In an attempt to perturb the electronic effects of the ruthenium catalysts, platinum was added as a second metal, since platinum is known to adsorb and activate H_2.[34] In CB–II–44 and 45, the ruthenium loading was 8% with 1% and 3.25% loadings of platinum, respectfully. As before, the maximum activity was observed at −158 °C with much less activity at −196 °C. In fact, β′ actually increased with respect to CB–II–20. However, there was β activity after reducing conditions and cooling in H_2. These results are shown in Table 15. This is thought to occur by a process similar to that described in the silicate section. Platinum particles partially cover some ruthenium sites; the Pt sites have less activity at −158 °C than Ru, causing β′ to increase. On the other hand, at −196 °C the Pt sites are more active following reduction without the He treatment, thereby causing β to decrease. Since neither β nor β′ showed dramatic improvements relative to previously established catalysts, the addition of platinum was not investigated further.

e. Effect of Catalyst Preparation Method

The Ru/SiO_2 catalysts discussed earlier were all prepared with the same general technique: Impregnation with ruthenium, removal of solvent with a rotovap at 50 °C, and drying overnight at 130 °C. This section will discuss modifications of that technique. Their effects on the subsequent activity are shown in Table 16.

CB–II–37 was prepared as CB–II–20 except the final drying was done under a room temperature vacuum instead of in an oven. Results remained consistent with what had been observed before. There was little activity at −196 °C following reduction and a β′ of 3.2 at

−158 °C (2). The "He Effect" was also observed, yielding a β^s of 15.8 (4). This value was closer to the β reported for CB−II−72 (16.6) which was prepared just like CB−II−20 and CB−II−24 (13.9) than that of CB−II−20 (8.5). To this date we were unable to determine the cause of this difference and are unable to prove or disprove any hypothesis as CB−II−20 was completely consumed during earlier testing.

As shown in Figure 12, there is a definite advantage to starting with a chloride containing ruthenium precursor. It was reported by Miura[35] along with Lu and Tatarchuk[36] that following reduction there was still residual chloride on the metallic Ru particles on the silica surface. Miura further reported that by washing the reduced catalyst in hot water and redrying, the chlorine is removed.[37] By washing CB−II−48, a catalyst prepared using $RuCl_3$, we expected a catalyst with properties similar to CB−II−29, which was prepared with $Ru(NO)(NO_3)_3$. This was confirmed by the observed "He Effect" β value of 34.7 (6), higher than the $\beta \approx 15$ values reported earlier for catalysts prepared with chloride containing precursors. Arguments about why residual chloride has an effect on the activity at −196 °C following "He Effect" activation will be presented later.

2. Ruthenium Ammine Precursor Catalysts

a. Activation Conditions

Catalysts were prepared by the general procedure described by Gay[28] and modified by Wu[29] with the preparation being reported elsewhere in this text. Gay described general activation conditions for reduction of ruthenium and desorption of the surface. The catalysts were reduced in flowing H_2 at 350 °C for 4 h. For desorption of the surface, the catalyst was heated at the same temperature for 12 h under a high vacuum In our case, the flowing He was used rather than a vacuum for simplicity.

b. General Procedures

Catalysts were prepared with $Ru(NO)(NO_3)_3$ as the precursor to the ammine with metal contents of 2%, 4%, 8%, 10%, and 12% by weight. However, due to the robust nature of the hydrazine reduction during the catalyst preparation, the higher ruthenium content catalysts were isolated with lower than expected metal contents. This was due to the splattering of the ruthenium solution on the sides of the beaker. Using the $KOH-KNO_3$ melt, an accurate metal content was obtained. The actual metal content was compared to the planned metal content and the difference was taken into consideration for future preps.

The catalysts were tested only for activity at −196 °C. While β' activity does exist for all catalysts, it occurred at a temperature greater than −160 °C, and an accurate temperature was not obtained. In most cases, the β' maximum activity was a much smaller increase over the β maximum, probably less than 20%. Due to these two factors, no β' values were reported.

c. Effect of Metal Content

The activities for catalysts prepared with $Ru(NO)(NO_3)_3$ are shown in Table 17. The values in the third column, $\beta^s[H_2]$, indicate activity following reduction and cooling in H_2, while those in the fourth column, $\beta^s[H_2-He]$, indicate reduction followed by desorption and cooling to −196 °C in He. As one can see, there is always an increase in activity upon heating and cooling in He over cooling in H_2, in other words, a "He Effect." The effect chlorine has on the "He Effect" will be discussed shortly. Table 17 also shows what effect metal content has on activity. With this preparation method, as little as 2% Ru can give a β value of 14. By increasing metal content, a β of 4 was obtained following H_2 /He activation. Additional ruthenium proved to be disadvantageous as the β value started to increase after a maximum metal content had been reached. This decrease in activity is shown in Figure 13, which displays the activity of all Ru catalysts prepared in this study. High activity can also

be measured if the catalyst is cooled in H_2 from the reduction temperature directly to −196 °C. "Flash Cooling" was done while testing CB−II−92,and a β of 3.3 was measured, which was even lower than that following He desorption. This technique was not attempted on other catalysts; it was done only to confirm if the "Flash Cooling" would work on this class of catalysts.

d. Effects of Precursor Metal and Preparation Method

Catalysts were also prepared using $RuCl_3$ and $Ru(NO)Cl_3$, respectfully. The metal content was intended to be 8% by weight, but varied due to the splattering problem described earlier. Activities for these catalysts are shown in the top two lines of Table 18. As one can see, catalysts prepared with a ruthenium chloride precursor had very low activity, even following He desorption of the surface. This would indicate that having chloride present while working up the catalyst modifies the surface in such a way as to deactivate the catalyst.

CB−II−89W was prepared by washing with hot water to remove residual chlorine. If the surface of CB−II−89 is similar to 88 and the only difference is the presence of chlorine; then by removal of chlorine, the activities should become similar. This is clearly not the case. As shown at the bottom of Table 18, activity decreases even more following this treatment. It would appear that the chlorine has to be either not present entirely or removed before the catalyst is dried/reduced.

CB−II−125 was prepared by the procedure described by Gay, without the modification described by Wu. The modification was to soak the support in ammonium hydroxide before introducing the reduced ruthenium solution. In the case of CB−II−125, the ruthenium was added to the support before reduction by hydrazine without soaking in ammonium hydroxide. It was stated by Gay that having the metal and support in contact during reduction would increase the metallic dispersion. The only exception to his procedure was that $Ru(NO)(NO_3)_3$ was used instead of $RuCl_3$. This eliminated the need to wash the wet catalyst with aqueous

ammonia to remove chloride.

CB–II–130 was prepared using the same technique as CB–II–125, except $RuCl_3$ was used. Because of this the catalyst was washed in cold 1M aqueous ammonia to remove chlorine. This experiment was performed to see if high activity at –196 °C existed if the chloride was removed prior to catalyst drying or final reduction.

As Table 18 illustrates, there is extremely high activity for CB–II–130 at –196 °C. Because this catalyst has a lower metal content relative to the catalysts prepared using $Ru(NO)(NO_3)_3$, it is felt that catalysts prepared taking advantage of this technique would have comparable activities to those prepared without chlorine being present altogether. This is an important fact should these catalysts be prepared commercially as the cost of $Ru(NO)(NO_3)_3$ is over twice that of $RuCl_3$.

3. (η^4–cyclohexa–1,3–diene)(η^6–benzene) Ruthenium (0) Precursor Catalysts

Results of the catalytic testing of catalysts prepared by the impregnation of (η^4–cyclohexa–1,3–diene)(η^6–benzene) Ruthenium (0) to a silica support is presented in Table 19. It is felt the following generalizations can be made about this class of catalysts. First, the β' activity changed very little with the percent metal loading or with the choice of activating gas. The temperature of maximum activity seemed to decrease slightly with increasing metal content. However, due to the inaccuracy of the measurement of that temperature, a strong conclusion cannot be made. Second, the β value at -196°C did show a definite decrease with increasing metal loading. It was also observed that the activity at -196 °C was generally greater when He instead of H_2 was used as the gas of activation. This is an expected result since the organometallic ruthenium precursor is already in a zero valent state and is deposited on the support following the thermal decomposition of the organic ligands. Helium is used to simply sweep these fragments along with any solvent away from the catalyst. The use of H_2 would achieve the same thermal decomposition of the precursor, but

the presence of H_2 may facilitate slight sintering of the catalyst, thus reducing the active surface area and activity. Another possible explanation is that of the H_2 poisoning of the catalyst as described in the previous sections. No attempts were made to activate the catalyst with H_2 followed by He as the organometallic ruthenium precursor work was completed before the H_2 poisoning was observed in the other catalysts.

C. Characterization of Ruthenium and Ruthenium Ammine Precursor Catalysts

1. H_2 Adsorption

When comparing the activity of traditionally prepared ruthenium catalysts with the ammine precursor catalysts, it was found that the latter catalysts had higher activity throughout the temperature range tested, but especially at −196 °C. It is felt that the major difference between these catalysts is the metallic dispersion. It has been previously stated that the ruthenium ammine precursor catalysts have high dispersions.[28] We wished to confirm this fact and see if any correlation existed between the dispersion and the catalytic activity, especially at −196 °C.

Table 20 displays the ruthenium metal dispersion for catalysts prepared with $Ru(NO)(NO_3)_3$ as a precursor to the ammine complex. As one can see, the dispersion is quite high for ruthenium supported on silica, generally over 20% regardless of metal content. The catalysts do show higher metallic dispersions at lower metal content, which is expected. The final column in Table 20 indicates the number of ruthenium atoms on the catalyst surface per gram of catalyst. This value is felt to be highly indicative of how active a catalyst is. The catalyst with the highest number of active metal sites on the surface should be able to convert the most H_2. However, since activity is measured by determining the weight of a catalyst needed to convert a known amount of H_2, the catalyst with the highest number of surface atoms per gram should be the most active.

Figure 14 is a plot of the activities of the catalysts in Table 20 vs. the total number of

ruthenium atoms per gram of catalyst; the triangles indicate catalysts prepared by ion exchange using $Ru(NO)(NO_3)_3$. As one can see, there is a definite correlation between the activity at −196 °C and the ruthenium surface atoms per gram catalyst. As expected, an increase in surface atoms generally means an increase in the catalytic activity. However, there does seem to be a slight decrease in activity with a large number of surface ruthenium atoms as well. One possible explanation for this is that a large number of surface ruthenium atoms also indicates a smaller ruthenium particle size. With the smaller particle size, there may be some geometric considerations with the adsorption and desorption of the reactant H_2 since the active sites will tend to be closer together. Another possible explanation is that smaller ruthenium particle will have a weaker interaction with an incoming H_2 molecule.[35] This may shorten the residence time of the H_2 on the surface, thereby decreasing activity. At this time, the cause of this observation is still undetermined.

The square marker in Figure 14 indicates CB–II–125, a catalyst prepared without using the ion–exchange method. As one can see, when the activity is plotted vs. the number of surface ruthenium atoms per gram, the catalyst fits in very nicely with the others, indicating there is little dependence upon the actual ammine precursor preparation technique.

Table 21 shows the dispersion of ammine precursor catalysts prepared using a chloride precursor. As shown in the first two entries, the use of a chlorine precursor definitely decreases the dispersion available through this technique. Since the activities of these two catalysts were also poor, β values of 42 and 61 for CB–II–89 and 93, respectfully, following H_2/He activation, it is felt that using a chloride precursor reduces dispersion greatly, hence decreasing activity. In other words, chlorine precursors make poor catalysts, especially with $RuCl_3$. However, since the dispersion of CB–II–93 is somewhat respectable, it is felt that residual chlorine may also decrease activity by an electronic effect as discussed earlier. The chlorine may weaken the Ru–H_2 interaction such that the mean lifetime of the adsorbed species is shortened so there is not adequate time for an o–p hydrogen interconversion to take

place.

The second two entries in Table 21 demonstrate attempts to remove chlorine from the catalyst. In CB–II–89W, in which chlorine was washed following drying and reduction, the dispersion and activity ($\beta = 45$) changed little. However, if chlorine was removed prior to drying as in CB–II–130, the dispersion and activity was as if a non–chlorine precursor was used. Activity vs. surface ruthenium atoms per gram for CB–II–130, plotted in Figure 14, is represented by a circle. As one can see, this catalyst fits in nicely with other catalysts prepared by different methods without chlorine. This result would support the earlier hypothesis that the presence of chlorine during the catalyst drying process causes the formation of a catalyst with poor dispersion.

For comparison, the metallic surface areas of selected traditionally prepared ruthenium catalysts were measured. These results are presented in Table 22. It is quite obvious that the metallic dispersions are much lower. This would indicate large particles and a smaller number of surface ruthenium atoms per gram of catalyst. This further supports the hypothesis that higher dispersions will yield higher activities.

An interesting observation is made when one compares the ruthenium atoms per gram of catalyst and the activity of the chlorine containing traditional catalysts to those of the chlorine containing ammine precursor catalysts. With the traditional chlorine catalysts, a H_2 /He activation β value of approximately 15 was obtained. However, with the ammine precursor chlorine catalysts, the H_2 /He activation β values were greater than 40. The ammine precursor chlorine catalysts were less active, even though there were a larger number of surface atoms per gram. This is a complete opposite to what was observed with the non–chlorine containing catalysts, both traditional and ammine precursor.

It is felt that this can be explained with the following argument. As discussed in earlier, the "He Effect" is caused by activated adsorption of H_2 followed by desorption with He. This is caused by the addition of electropositive chlorine on a large ruthenium particle.

Since the ruthenium particle is large, the chlorine is not felt to be a geometric hinderance to incoming H_2, yet it can still cause an electronic effect.

However, in the case of the ammine precursor catalysts, it is a different story. Even though the catalysts have a greater number of surface ruthenium atoms, the "He Effect" activity is less than for a traditional catalyst. Reasoning behind this is two-fold. First, for the ammine precursor catalysts, a higher dispersion means smaller ruthenium particle size. This means the residual chlorine is sitting on a much smaller ruthenium particle. In this case it is more likely to be deactivating the catalyst through a geometric pathway. The chlorine simply blocks the path of the incoming H_2 to the surface. Second, with a smaller metal particle, Lu and Tatarchuk stated that the chlorine electronic effects with the metal would be greater. Knowing this, it is possible that the interaction between the incoming H_2 and the activated Ru would be lessened, especially at low temperature. This would cause the H_2 residence time to decrease, decreasing activity. At the present time it is not known if one, or both, of the above hypothesis are responsible for the above observations.

2. Low Temperature Susceptibility

Low temperature magnetic susceptibilities of selected catalysts were valuable in explaining the behavior of different ruthenium catalysts. Without these data, the previous assumptions with respect to β' could not have been made. A much simpler hypothesis to explain why ruthenium catalysts show a maximum activity would be that the magnetic susceptibility of the catalyst varies with temperature. It reaches a maximum value at a temperature corresponding to the temperature of maximum catalytic activity. This maximum susceptibility would then decline to −196 °C. It was therefore necessary to measure the magnetic susceptibilities vs. temperature of various catalysts to see if any maxima exist, which would support the above hypothesis.

The first catalyst tested was AP. It was tested following activation at 200 °C for 2 h

in a He flow. The magnetic susceptibility was plotted vs. temperature in Figure 15. This experiment displays that the magnetic susceptibility of the catalyst increases with decreasing temperature. This is what is expected for a paramagnetic metal. Further evidence for the paramagnetic character of this catalyst is shown in Figure 16. For a paramagnetic species, the plot of the inverse susceptibility vs. temperature should be linear.

As shown in Figure 15, the magnetic susceptibility nearly doubles over the temperature range studied. However, if one looks at the plot of activity vs. temperature over the same range, there is little change in activity. In fact, any difference displayed in activity would be opposite of what would be predicted solely by using susceptibility. This implies that there are other factors which outweigh the effects of the magnetic susceptibility.

Ruthenium catalysts were the next to be tested. The magnetic susceptibility of CB–II–24 without activation is shown in Figure 17. As one can see, the magnetic susceptibility is completely different. First, the catalyst showed a diamagnetic behavior, meaning the catalyst was repelled by the applied magnetic field. Also, the calculated magnetic effect was approximately two orders of magnitude smaller than that calculated for AP. Finally, there is little variation of the magnetic susceptibility with change of temperature. The small variation found occurred at temperatures closer to −196 °C, where the catalyst appeared to be less diamagnetic.

The temperature dependence of the magnetic susceptibility of CB–II–24 following reduction at 350 °C in H_2 is shown in Figure 18. This experiment was done to determine if magnetic susceptibility would change by changing the oxidation state from Ru^{III} to Ru^0. As shown, the curve of Figure 18 is very similar to Figure 17. The only difference is that the reduced catalyst had a smaller diamagnetic effect. It is felt that this is simply caused by the catalyst having a higher weight percent of Ru following reduction.

For comparison, other ruthenium catalysts prepared by Fubara[38] and Wang[39] were tested. These catalysts were all Ru^0 catalysts, but prepared by different methods. In Figure

18, the magnetic susceptibility of BF–40Cl is shown. This was a ruthenium catalyst with a 24% Ru metal loading, supported on alumina. Catalytic properties of this catalyst were very similar to the traditionally prepared ruthenium catalysts, with a β value of 5.7 following reduction at 400 °C and a β' of about 1 at −154 °C. It is interesting that this catalyst showed a positive paramagnetic response at temperatures lower than −160 °C, but was slightly diamagnetic at temperatures greater than −160 °C. Once again, the order of magnitude of the measured magnetic susceptibility is over a hundred times less than that of AP.

The magnetic susceptibility of WW–17 (5.7% Ru/SiO_2) is shown in Figure 20. This catalyst was prepared by the impregnation of the organometallic compound (η^4–cyclohexa–1,3–diene)(η^6–benzene)ruthenium(0) onto a silica support. The aim of this work was to impregnate a Ru^0 source and achieve an active metal by pyrolyzing the catalyst in N_2. The activity of this catalyst was very similar to traditional catalysts with a β value of 43.4 and β' of 2.85 at −154 °C. This was following H_2 activation at 400 °C for 4 h. The major differences between this catalyst and other Ru catalysts tested is that a paramagnetic response is shown. This response varied little throughout the entire temperature range measured.

3. X-ray Diffraction

In an attempt to further characterize the ruthenium catalysts, X–ray diffraction powder patterns were collected. The reasoning behind this was two fold. First, we wanted to establish chemical purity of the samples. X–ray diffraction can be used as an analytical tool to fingerprint various components of a catalyst. Second, one can use the line broadening of selected peaks to determine the metallic particle size. This information was helpful to determine if there was good dispersion of the ruthenium, as smaller particles lead to higher dispersions. These experiments were especially important before the capability to do active gas chemisorption was obtained. With regard to catalyst purity, we wished to look at a

catalyst following reduction to determine what metallic phases remained. This was important to determine which oxidation state of ruthenium was active for *ortho*– to *para*–H_2 conversion; and if one particular state was active at one temperature while a different state was responsible for activity at another temperature. Before catalyst X-ray diffraction patterns (XRD) could be collected, the XRD's of ruthenium compounds which could possibly remain following reduction needed to be established as standards.

Figure 21 shows the XRD for ruthenium metal following the reduction of $RuCl_3$ at 650 °C in H_2. The reduction temperature was high to promote large particle growth. As one can see, there are 6 major lines between 30 and 80 degrees, with the most intense line at 44 degrees.

Figure 22 displays the XRD for RuO_2, prepared by air–oxidation of ruthenium metal at 650 °C. The RuO_2 is much more complex, with its most intense lines at 35 and 54 degrees, respectfully. The small lines around 44 degrees are believed to be remaining Ru metal.

Figure 23 displays the XRD for $RuCl_3$. The pattern is less sharp because the sample was prepared without heating and was dried under vacuum before the pattern was collected. This pattern shows the most intense peak at 44 degrees, which is the same as the most intense peak for ruthenium metal. In fact, all the peaks match those seen in the ruthenium sample except for 35 degrees, which matches the most intense peak for RuO_2. Therefore, it is difficult to determine the presence of $RuCl_3$ by XRD alone.

The XRD of CB–II–46 following reduction at 450 °C is shown in Figure 24. Several important features of this XRD are noteworthy. The 6 lines all match lines found in the pure ruthenium sample. There was no line at 35 degrees which would indicate RuO_2. Second, the lines all show some degree of line broadening when compared to ruthenium metal. In fact, the particle size was determined using the line at 44 degrees to be ~9.5 nm. Using the formula (Dispersion=1/Particle Size), the metallic dispersion can be estimated at 10.5%. This

value is much higher than discussed earlier in this chapter. It is felt that this is due to a combination of factors. First, there is probable error in the particle size estimation by XRD line broadening. Usually, the estimate is good to within an error of ±30%. Second, there is a better chance of error in the adsorption studies when a low metallic dispersion is being measured. Most likely, the weakly bound H_2 was overestimated because of the relatively small amount of chemisorbed H_2. This overestimation would lead to the calculation of a dispersion lower than the actual value.

Figures 25 and 26 show CB–II–48 following reduction at 450 °C and following hot water wash and re–reduction at the same temperature. One can easily see that the XRD's are nearly identical, indicating there was little change in the surface structure following hot water wash. This supports the previous claim that any "He Effect" activity lost is due to removed chlorine and not from other surface changes. The particle size was determined by line broadening to be 7.5 nm, and the dispersion was 13.5%, both expected changes from CB–II–46 since metal content was decreased.

D. Discussion and Conclusions of Ruthenium Catalysts

1. Hypothesis for Activity > -196 °C

To help us understand why one particular catalyst would have an optimum temperature of enhanced activity, and a lower temperature with almost no activity, one must look at the basic process occurring during an *ortho*– to *para*–H_2 transition.

For a gas–phase *ortho*–H_2 to be converted to a gas–phase *para*–H_2, it first must be adsorbed on the catalyst. For this, there is a corresponding rate constant and change in enthalpy (ΔH) of adsorption. For the adsorption of H_2 on Ru, especially at low temperatures, it is felt that this process goes fast and involves a fairly strong interaction with the surface. Secondly, the *ortho*–H_2 adsorbed on the surface must have a sufficiently long residence time

to undergo nuclear spin flip required for conversion to *para*–H_2 adsorbed on the surface. Finally, this adsorbed *para*–H_2 must desorb from the surface to a gas–phase *para*–H_2. The desorption process has a rate constant associated with it as well. This complete process is shown schematically in Figure 27. Since the adsorption of H_2 at low temperatures on a Ru surface is fast, one can eliminate the first step as a factor. The second step, however is of particular interest. It is known that as the temperature is lowered, the residence time of an adsorbate on the surface increases.[40] At a certain temperature, the H_2 will remain on the surface for an optimal conversion time, followed by its desorption. But at lower temperatures, the H_2 will remain adsorbed on the surface even longer following conversion from *ortho*– to *para*–H_2. This blocks the path for other gas–phase reactant *o*–H_2 to get to the surface. It is felt that these molecules will adsorb as a subsequent layer atop the pre–existing first layer. But as shown previously in the theoretical calculations for this reaction, an increase in the radius of reactant H_2 molecules to the active metal by the adsorbed layers, will cause an exponential decrease in the conversion for the upper layers.

It is felt that this same hypothesis applies for the silicate chemistry as well. However, since the ΔH of adsorption is less for the metals in which silicates were prepared (Ni, Fe, Mn), the residence time will be shorter than those associated with Ru at the same temperature. In fact, it is quite possible that at a temperature lower than −196 °C, there will be a maximum activity, as displayed for the Ru catalysts. However, since this study does not allow for testing at temperatures colder than −196 °C, data which might support this hypothesis were not available.

2. Hypothesis for "He Effect" Activity

The above explanation rationalizes why a traditional ruthenium catalyst will show a maximum activity at a given temperature and how it is related to the rate of desorption of the converted H_2 along with the ΔH of adsorption. A similar phenomenon can

help to explain why there is enhanced activity after the heating in He and the cooling to −196 °C in He as well as cooling directly from the reduction temperature to −196 °C.

It is well known that H_2 will irreversibly and dissociatively adsorb on Ru at room temperature.[35,41,42] This adsorption has a relatively large ΔH of adsorption. Following reduction and as the catalyst cools to room temperature, the surface will be completely covered by a H_2 layer. Therefore, for any *ortho*−H_2 to be converted to *para*−H_2, it has to physisorb on the surface of the chemisorbed layer as a second layer. This can also be considered as reversible H_2 which adsorbs onto the irreversibly adsorbed layer. As one lowers the temperature from 23 °C. The gas−phase H_2 will start to increase its residence time on the *nth* layer of H_2 instead of the metal surface.

However, if one heats in He and then cools in He to −196 °C in the same gas, the activity is enhanced, and one can be assured that the catalyst surface is clean of any adsorbed gases, including H_2. Following cooling in He and the introduction of reaction H_2 at −196 °C, there will be adsorption on the surface. However, since the sample is at cryogenic temperatures, the only H_2 adsorbed will be that with a low ΔH of adsorption. There is not enough energy in the system to furnish the activation energy for chemisorption which gives the irreversible H_2 with a large ΔH. This should help to lower the distance from the outer layer to the surface, thus increasing activity. This is shown visually in Figure 28a, where a rectangle indicates a layer of adsorbed H_2.

It has been shown in Figure 12 that residual chlorine on the catalyst surface can increase the effectiveness of the He effect. Lu and Tatarchuk have shown that residual chloride attached to ruthenium particles on the surface will cause activated H_2 adsorption,[35] meaning the ΔH for dissociative adsorption is increased for those catalysts containing residual chlorine. For H_2 to dissociatively adsorb on ruthenium, there has to be a donation of electrons from ruthenium to hydrogen. However, since chlorine is electronegative, it withdrawals electron density from ruthenium. This makes the formation of the Ru−H bond

more difficult, thus requiring a higher energy of activation. This has little effect on a catalyst cooled from the reduction temperature to room temperature in H_2. At the higher temperatures of reduction, there is sufficient energy for adsorption and the surface is covered as before. However, following the H_2 /He activation, since the ΔH for H_2 adsorption is higher, there should be less H_2 adsorbed on the surface than compared to a ruthenium surface without chlorine present. This lowers the distance to the surface for a gas–phase H_2 and should increase activity. A catalyst with residual chloride is portrayed following cooling in H_2 and H_2 /He activation in Figure 28b.

A similar phenomenon occurs when the catalyst is "Flash Cooled", meaning the catalyst is cooled directly from reduction temperature to −196 °C using a liquid nitrogen bath. At the high reduction temperatures, there is very little H_2 adsorbed on the catalyst surface. H_2 is known to form a very strong interaction with ruthenium at room temperature or warmer, but by cooling directly to −196 °C the H_2 is not allowed enough time to interact and be strongly adsorbed with the ruthenium surface, thereby creating the same situation as discussed in the "He Effect" and portrayed in Figure 28b.

3. Conclusions for Ruthenium Catalysts

While comparing the catalyst prepared with a ruthenium ammine precursor to those prepared with traditional metal precursors, there are two glaring differences. The ammine catalysts which started from $Ru(NO)(NO_3)_3$, had much greater activity than their corresponding traditional preparation counterparts. This was true for testing after reduction and cooling in H_2 as well as reduction in H_2 and desorbing/cooling in He. Second, there was no enhancement following He desorption/cooling for ammine catalysts starting with a metal chlorine precursor. In fact, the ammine catalysts starting from a ruthenium chloride source lost considerable activity compared to the non-chlorine counterparts under the differing activation conditions. The only catalyst prepared with a chlorine precursor which had good

activity was CB–I–130 in which the chlorine was removed prior to drying of the catalyst.

When asking the question of why the two preparation methods yield such different results, one must look at the basic differences between the two. It is known that traditional Ru catalyst have relatively low surface areas, usually with a maximum dispersion of 0.2 at low metal loadings.[40,43] Dispersions for these ammine catalysts have exceeded 0.3 with dispersions up to 0.6 to 0.8 reported for catalysts with lower metal loadings. It is felt that with the higher dispersions possible using an ammine precursor, more active sites are available per unit mass, to convert more *ortho*–H_2 to *para*–H_2. Even though there is a "He Effect" on the ammine catalysts, which indicates that H_2 poisoning is occurring on the surface, there are more active sites on the ammine catalyst's surface to get poisoned. If the surface of an ammine catalyst is poisoned the same amount as a traditional catalyst, the ammine catalyst should have a higher activity due just to more active sites. This discussion of activity increasing with higher dispersion would suggest that *ortho*– to *para*–H_2 interconversion is a structure sensitive reaction, meaning the rate of the reaction is directly related to the changes in particle size and dispersion.

The addition of chlorine via the use of a chloride containing precursor completely deactivates the catalyst. Removal of chlorine using a hot water wash has little effect on this deactivation. Alternatively, if the chloride is removed prior to the drying of the catalyst, the activity is the same as if the chlorine was never present.

There are several possible arguments to explain the observation. Lu and Tatarchuk state that there are two possible reasons that chlorine may act to cause activated adsorption.[35a] Since the formation of a Ru–H bond requires donation of electrons from the Ru to the gas–phase H_2, electronegative chlorine will cause a decrease in the local electron density of the ruthenium, thereby increasing the activation energy to form that bond. Alternatively, the chlorine may act as a geometric barrier in which it inhibits the surface movement of H_2 and imposes a kinetic barrier on the adsorption process.

In the case of the traditional preps, it was stated earlier that an electronic effect is occurring. A small chlorine atom is sitting on a much larger Ru cluster that is perturbing the electronics, but not blocking the path of a H_2 to an active sites. In the case of the more highly dispersed ammine catalyst, the geometric explanation is more logical. A chlorine sits on a much smaller Ru cluster, thereby blocking most of the ruthenium sites from the H_2.

Lu and Taterchuk also stated that the electronic effects were more pronounced for a more highly dispersed surface.[35b] Another possible explanation is that the activation energy becomes too great for an interaction between the surface and a reactant H_2. Without a surface interaction, the distance between the surface and H_2 would be large, decreasing activity.

A third possible alternative explaination would be that the presence of chlorine during the drying process causes the formation of a very poor catalyst, one with a very low metallic surface area. This will be discussed in more detail within the next section.

4. Conclusions of Physical Characterization

Conclusions made from the active gas adsorption study are: 1) The dispersion of the ammine precursor catalysts without chlorine are greater than traditional catalysts, independent of preparation technique; 2) The ammine chlorine precursor catalysts have decreased dispersions and decreased activities, relative to all catalysts; 3) The traditional catalysts, both with and without chlorine, have further decreased dispersions but activities greater than ammine chlorine precursor catalysts; 4) For the ammine precursor catalysts, if chlorine is removed prior to drying, the catalyst is as active as the non–chlorine catalysts.

Several conclusions can be made from the low temperature magnetic susceptibility studies. First, there is little variation of magnetic susceptibility with temperature for ruthenium catalysts. Second, bulk ruthenium catalysts can show diamagnetic behavior. Third, for the most part ruthenium catalysts showed lower magnetic susceptibilities than nickel silicate. Finally, there is little correlation between a high magnetic susceptibility and

high activity. Therefore, it was concluded that magnetic susceptibility is not a major factor in determining catalytic activity or helping to explain β.

Several conclusions can be made from the XRD study. The metal ruthenium was determined to be the major, (if not the only) oxidation state of ruthenium present in the catalysts tested. The ruthenium lines of a reduced catalyst were broadened, indicating smaller particle sizes. The amount of this broadening was dependent upon metal loading. Dispersions calculated from these particle sizes were higher than by other methods, most likely due to interference caused by the silica support.

IV. CONCLUSION

The main goal of this study was to develop and improve on existing catalysts for the conversion of *ortho*– to *para*–hydrogen. Starting with a commercially available Air Products nickel silicate, which had a β value of 20, we were trying to synthesize catalysts that would be an improvement to AP. This was accomplished by preparing silicates with various metals as well as different preparation methods. We also prepared supported ruthenium catalysts by various techniques using several metal precursors to improve present technology. What was also found was that the activation conditions prior to catalytic testing was highly important for both the silicates and the supported ruthenium catalysts.

While not the initial focus of the research, we made some interesting observations into the adsorption of H_2 on ruthenium. This helped us to get a better understanding of how *ortho*– to *para*–H_2 conversion takes place, and what features in a catalyst are important to optimize activity.

Reactor design was the final area in which some interesting conclusions were drawn. As discussed earlier, the reactor catalyst bed must be constructed using straight 1/8" OD stainless steel tubing. It was determined that the use of 1/4" OD tubing caused two problems. First, the radius from the center of the bed to the wall was too great for thermal equilibrium. Since the reaction of *ortho*– to *para*–H_2 is exothermic, the catalyst bed center was warmer than the edges. Second, the catalyst bed was too shallow using a 1/4" tube. This caused reactant blow–by which was thought to decrease the measured activity when the flow rate was increased. The 1/8" tube corrected both of these concerns.

While preparing and testing the transition metal silicates, some interesting conclusions were drawn. It was first concluded that nickel was the best candidate for preparing metal silicates. All other metal silicates had much lower activities relative to AP nickel. It was also observed that by increasing the catalyst activation temperature in He from 150 °C to 300

°C, and by decreasing the activation time from 4 h to 2 h, the β decreased from 20 to 15.7. By refluxing in 2,2–DMP, a β of 16 could be achieved in 40 min. It is felt that the increased activity is the result of increased dehydration of the catalyst. This can increase activity in two possible ways. First, increased dehydration causes decreased catalyst weight, which would essentially mean there are more active sites per unit mass. Second, by removal of adsorbed water, the H_2 would have a clearer path to an active site. The H_2 molecule should also have a shorter distance to an active site, which should increase activity.

It was also concluded that an increase in the total pore volume and total surface area of a silicate correspond to an increase in activity. Subsequent modifications in the catalyst prep, which included washing and refluxing the catalyst in MeOH, as well as preparing the catalyst in an ethylene glycol solution, all increased total pore volume. The β value decreased from 17.1 to 11.0 following all modifications. The increase in pore volume is thought to promote the mass transport of H_2 through the catalyst particle, which should increase the ease of a reactant H_2 molecule to reach the surface and be converted. An increase in total surface area could increase the number of active sites which in turn, should increase activity.

However, that ruthenium supported on silica was the most active catalyst for the conversion of *ortho*– to *para*–H_2. Following reduction for 4 h at 450 °C in H_2, it was found that a β′ of 3.3 at −158 °C was obtained. This activity varied slightly with metal precursors. The catalysts prepared using a ruthenium precursor containing chlorine were slightly more active than those prepared without chlorine. The activity also varied with metal content. The activity increased with increasing metal content for all catalysts, until a maximum metal content was achieved. It is believed that the maximum metal loading is between 8 and 10 percent by weight.

As stated before, the activity was dependent upon the activation conditions. By heating the catalyst in He following reduction and by cooling the catalyst to −196 °C in He

prior to H_2 introduction, a β value of between 8 and 15 was obtainable for traditional ruthenium catalysts prepared using a metal precursor containing chlorine. For a catalyst prepared with a non–chlorine containing precursor, or a catalyst in which the chlorine was washed out, the "He Effect" β increased by up to a factor of 4.

As stated earlier, there are two hypotheses which explain why the traditional ruthenium catalysts have an optimal temperature for maximum *ortho*–H_2 conversion, and why there is a "He Effect" and why chlorine containing precursors give increased H_2 /He activation activity. The maximum activity at an optimal temperature is believed to be controlled by the rate of desorption of an H_2 molecule after it has been converted from the *ortho*–H_2 to *para*–H_2 form. It is felt that the residence time of the adsorbed H_2 molecule increases as the temperature decreases. At a certain temperature, –158°C for the traditional ruthenium catalysts, there is an optimal residence time for conversion from *ortho*– to *para*–H_2. As the temperature decreases and the residence time increases, it is felt that the adsorbed *para*–H_2 blocks the path to the surface for incoming *ortho*–H_2 and subsequently lowers the rate of conversion and activity of the catalyst.

The "He Effect" is believed to be simply caused by an adsorption/desorption phenomenon of the reactant hydrogen. H_2 is known to disassociatively chemisorb on ruthenium at room temperature. The heating of the catalyst to 350 °C or greater in He will desorb the surface of chemisorbed H_2; by cooling to –196 °C in He prior to reactant H_2 exposure will help to keep the irreversible chemisorption of H_2 to a minimum. This will reduce the distance for an incoming H_2 molecule to the surface, which should increase the rate of conversion.

The use of a chlorine containing ruthenium precursor increases the "He Effect" by the presence of residual chlorine on the catalyst surface following reduction. Residual chlorine, an electronegative element, is known to withdraw local electron density from the ruthenium surface. Since the disassociative chemisorption of hydrogen requires the donation of electrons

from the surface ruthenium to the hydrogen to form a Ru–H bond, the presence of chlorine should increase the activation energy and make that Ru–H bond harder to form. Therefore, following the H_2 activation and after the catalyst has been cooled to –196 °C in He, it should be even harder to form a Ru–H bond. This should lower the number of chemisorbed hydrogens on the surface and increase the rate of *ortho*– to *para*–H_2 conversion at –196 °C. This is caused by the decrease in the distance between a gas–phase H_2 molecule and the surface, as well as open more active sites for physisorption.

Another class of ruthenium catalysts were prepared, this time through the impregnation of a Ru^{II} ammine complex, prepared by the hydrazine reduction of various previously used ruthenium salts. This preparation technique is known to create a highly dispersed ruthenium surface, something that is known to be hard to accomplish on silica support by standard impregnation techniques and with common ruthenium precursor salts.

The activity at –196 °C of the ammine precursor catalyst class, in which the ruthenium ammine was prepared using $Ru(NO)(NO_3)_3$, was greatly increased, as was the metallic dispersion of the catalysts when compared to other traditional ruthenium catalysts preps. This catalyst class was highly active following both the normal reduction and cooling in H_2, as well as following the H_2 /He activation. Since this class of catalyst is more highly dispersed, there are more active sites available for *ortho*– to *para*–H_2 conversion, thus causing an increased "He Effect". This increased dispersion will affect the activity of a catalysts in which there was no H_2 desorption prior to testing. Since there is a higher dispersion, there will be a greater number of "H_2 poisoned" ruthenium sites than a similar catalyst prepared with traditional impregnation techniques. If the degree of poisoning is consistent for both classes of catalysts, the ammine precursor catalysts should have higher activity, and experimentally, this is the case.

The increased dispersion also affected the measurement of β'. As noted earlier, the difference between the maximum detector response and the detector response at –196 °C was

normally less than a 20% increase. It is also felt that the temperature at which this maximum *ortho*–H_2 conversion occurs is at a temperature lower than the –158 °C measured for a traditional catalyst. It would appear that the smaller ruthenium particle size that is associated with a more highly dispersed surface, decreases the temperature at which there is an optimal hydrogen residence time on the surface for *ortho*– to *para*–H_2 conversion. However, since this temperature is colder than –160 °C, an accurate temperature was not recorded.

With traditional ruthenium catalysts, it was found that the use of a chlorine containing ruthenium precursor increased the catalytic activity at –196 °C. This was not the case, however, for ruthenium catalysts prepared through the ruthenium ammine precursor intermediate. It was found that the activity at –196 °C, as well as the activity at temperatures warmer, dropped dramatically from the other ruthenium ammine precursor catalysts prepared with a non–chlorine containing precursor. If the chlorine was remove prior to catalyst drying and reduction, the catalyst was as active as if chlorine was never present. But if chlorine was removed following the drying/reduction of the catalyst, the activity was poor. There are several possible explanations for this. First, the chlorine can block the path of reactant H_2 to the surface. This effect would be more pronounced for the smaller particles of a more highly dispersed surface. Second, smaller ruthenium particles can increase the effect of chlorine on the Ru–H interaction. It may weaken the interaction such that the residence time for a reactant *ortho*–H_2 molecule is short so that the H_2 is not on the surface long enough for conversion to take place. Finally, the presence of chlorine while preparing an ammine precursor catalyst makes a poor catalyst.

In this study, we were able to understand some of the properties in catalyst preparation as well as catalyst activation conditions that yield high rates of *ortho*– to *para*–H_2 conversion. From the study of both metal silicates and impregnated ruthenium silica catalysts, it was concluded that catalytic activity increased with the total number of active sites. With the ruthenium catalysts, information about the properties of H_2 adsorption on a

ruthenium surface, as well as the effect of residual chlorine on this adsorption process were ascertained by the study of catalytic activity. Further investigation into this topic may include optimizing the preparation method of the ruthenium ammine precursor catalyst, as well as further investigation into the ammine precursor catalysts by physical characterization.

Table 1. Impregnation of Air Products by $Fe(NO_3)_3$

Sample	Metal Conc.	Impregnation Time
CB–I–18	0.1 M	4 h
CB–I–19	0.2 M	4 h
CB–I–20	1.0 M	2 h
CB–I–21	1.0 M	12 h
CB–I–24	0.2 M	20 min
CB–I–25	0.5 M	2 h
CB–I–27	0.1 M (MeOH)	2 h
CB–I–28	1.0 M (MeOH)	2 h
CB–I–22	1.0 M $Cr(NO_3)_3$	2 h

Table 2. Impregnation of $Fe(NO_3)_3$ on CB–I–9M

Sample	Metal Conc.	Impregnation Time
CB–I–14	0.1 M	2 h
CB–I–15	0.2 M	2 h
CB–I–16	0.3 M	2 h
CB–I–17	0.4 M	2 h

Table 3. Activity of Air Products Nickel Silicate

Catalyst	Activation Conditions Time	Temperature	Gas	β^s value
AP	4 h	150 °C	He	20.0
AP	12 h	150 °C	He	24.0
AP	2 h	275 °C	He	15.7
AP	2 h	150 °C	H_2	> 100
AP	2 h	300 °C	H_2	> 100
AP	2 h	275 °C	Vacuum	16.0

β^s = is single point determination at −196 °C

Table 4. Activity of Enhanced Air Products

Catalyst	Activation Conditions Time	Temperature	β^s Value
AP	2 h	275 °C	15.7
AP–DMP	40 min	275 °C	16.1
AP–DMP	0 min	23 °C	40.0
AP	0 min	23 °C	> 100
AP–M	2 h	275 °C	16.2
AP–R	2 h	275 °C	16.2

All tested with He Activation

Table 5. Iron, Chromium and Manganese Silicates

Catalyst	Metal	β^s Value
CB–I–1	Fe	49.2
CB–I–2	Fe	> 100
CB–I–3	Cr	> 100
CB–I–4	Cr	> 100
CB–I–13	Mn	20.7

150 °C for 4 h in He

Table 6. Activity of Nickel Silicates

	Activation Conditions		
Catalyst	Time	Temperature	β^s Value
CB–I–7	4 h.	150 °C	55
CB–I–9	4 h.	150 °C	60
CB–I–9	2 h.	275 °C	17.1
CB–I–9M	4 h.	150 °C	14.4
CB–I–9M	2 h.	275 °C	13.3
CB–I–9MR	1/2 h	300 °C	12.1
DML–EG	2 h	275 °C	11.0

Table 7. Activity for Fe (Cr) Impregnated on Air Products

	Activation Conditions		
Catalyst	Time	Temperature	β^s Value
Air Products	2 h	275 °C	15.7
CB–I–18	2 h	260 °C	24.3
CB–I–19	1 h	260 °C	24.2
CB–I–20	1 h	260 °C	75
CB–I–21	1 h	260 °C	40
CB–I–27	1 h	225 °C	60
CB–I–28	1 h	260 °C	22
CB–I–22 (Cr)	1 h	260 °C	37

Table 8. Activity of Fe Impregnated on CB–I–10M

Catalyst	Activation Conditions		β^s Value
	Time	Temperature	
CB–I–9M	2 h	275 °C	13.3
CB–I–14	45 min	260 °C	10.2
CB–I–15	45 min	260 °C	10.4
CB–I–16	45 min	260 °C	10.7
CB–I–17	45 min	260 °C	27.3

Table 9. Surface Area and Pore Volume Measurements for Selected Metal Silicate Catalysts

Catalyst	Metal	Surface Area (m^2/g)	Pore Volume (cc/g)
CB–I–1	Fe	---	---
CB–I–3	Cr	125.0	---
CB–I–4	Cr	85.7	---
CB–I–13	Mn	225.0	0.55
CB–I–9	Ni	250.2	0.231
CB–I–9M	Ni	397.0	0.397
CB–I–9MR	Ni	474.5	0.440
DML EG	Ni	---	0.616
CB–I–12	Fe/Ni	195.8	---
AP	Ni	416	0.65

Table 10. Activity of CB–II–20; 8.04% Ru/SiO_2 $RuCl_3$ Precursor

Activation Conditions				Test Conditions				
Time	Temp	Gas	Pressure	β^s	β^m	β'	Pressure	Trial
4 h	335 °C	H_2	20 psi	100	---	3.8	200 psi	1
12 h	335 °C	He	20 psi	100	---	6.7	200 psi	2
4 h	450 °C	H_2	20 psi	100	---	3.3	200 psi	3
4 h	550 °C	H_2	20 psi	100	---	3.9	200 psi	4
4 h	450 °C	H_2	200 psi	100	---	3.4	200 psi	5
4 h	335 °C	H_2	200 psi	100	---	3.8	200 psi	6
4 h	450 °C	He	20 psi					
4 h	450 °C	H_2	20 psi	100	---	3.5	200 psi	7
4 h	335 °C	H_2	20 psi	100	---	3.8	300 psi	8
4 h	335 °C	H_2	20 psi	100	---	3.8	400 psi	9
4 h	335 °C	H_2	20 psi	100	---	3.8	500 psi	10
4 h	450 °C	He	20 psi					
12 h	225 °C	H_2	20 psi	100	---	3.2	200 psi	11
8 h	450 °C	H_2	20 psi	100	---	3.2	200 psi	12
8 h	450 °C	H_2	20 psi					
12 h	450 °C	He	20 psi					
5 min	-196 °C	He	20 psi	8.5	---	2.8	200 psi	13
1 h	23 °C	H_2	20 psi	36.1	---	3.5	200 psi	14

Table 11. Activity of CB–II–72

Activation Conditions				Test Conditions				
Time	Temp	Gas	Pressure	β^s	β^m	β'	Pressure	Trial
4 h.	450 °C	H_2	20 psi	45	---	5.9	250 psi	1
Iso-pentane slurry				---	---	3.7	250 psi	2
4 h.	450 °C	H_2	20 psi					
Cooled at 100 °C in H_2				43.4	---	6.9	250 psi	3
4 h.	450 °C	H_2	20 psi					
Cooled at 350 °C in H_2				30.8	44.0	5.9	250 psi	4
20 h.	450 °C	H_2	20 psi					
Cooled at 350 °C in H_2				40.6	55.3	5.2	250 psi	5
4 h.	450 °C	H_2	20 psi					
1.5 h.	450 °C	He	20 psi					
5 min.	-196 °C	He	20 psi	16.6	26.0	5.4	250 psi	6

β^s indicates single point measurement at -196°C
β^m indicates multi point measurement at -196°C
β' indicates single point measurement at -158°C

Table 12. Activity of Catalyst prepared with $RuCl_3$ Precursor

Activation Conditions				Test Conditions					
Time	Temp	Gas	Pressure	β^s	β^m	β'	Pressure	CB–II–#(Wt%)	Trial
4 h	325 °C	He	20 psi	100	---	100	200 psi	15 (0.1)	1
4 h	450 °C	H_2	20 psi	100	---	100	200 psi	15 (0.1)	2
18 h	325 °C	He	20 psi	100	---	25.9	200 psi	18 (1.1)	3
5 h	275 °C	H_2	20 psi	100	---	4.9	200 psi	18 (1.1)	4
4 h	450 °C	H_2	20 psi	100	---	5.0	100 psi	18 (1.1)	5
4 h	450 °C	H_2	20 psi	100	---	5.0	100 psi	8A (1.9)	6
12 h	325 °C	He	20 psi	100	---	6.7	200 psi	14 (2.6)	7
5 h	450 °C	H_2	20 psi	100	---	3.9	200 psi	14 (2.6)	8
12 h	325 °C	He	20 psi	100	---	7.4	200 psi	19 (4.4)	9
5 h	450°C	H_2	20 psi	100	---	4.0	200 psi	19 (4.4)	10
8 h	450 °C	H_2	20 psi						
12 h	450 °C	He	20 psi						
5 min	-196 °C	He	20 psi	36.0	52.1	6.6	200 psi	19 (4.4)	11
1 h	23 °C	H_2	20 psi	75.0	---	8.8	200 psi	19 (4.4)	12
5 h	450 °C	H_2	20 psi	>75	---	3.7	200 psi	46 (14.5)	13
15 h	450 °C	H_2	20 psi	35	---	3.5	200 psi	46 (14.5)	14
2 h	450 °C	He	20 psi						
8 h	450 °C	H_2	20 psi						
12 h	450 °C	He	20 psi						
5 min	-196 °C	He	20 psi	15.2	17.4	---	200 psi	46 (14.5)	15

Table 13. Activity of Ru/SiO_2; $Ru(NO)Cl_3$ Precursor

Acitvation Conditions				Test Conditions					
Time	Temp	Gas	Pressure	β^s	β^m	β'	Pressure	CB–II–#(Wt%)	Trial
5 h	450°C	H_2	20 psi	100	---	6.1	200 psi	21 (1.1)	1
5 h	450°C	H_2	20 psi	100	---	3.7	200 psi	22 (3.2)	2
5 h	450°C	H_2	20 psi	100	---	3.8	200 psi	23 (5.9)	3
5 h	450°C	H_2	20 psi	>75	---	4.1	200 psi	24 (9.2)	4
4 h	450°C	H_2	20 psi						
2 h	450°C	He	20 psi						
5 min	−196°C	He	20 psi	13.5	19.3	4.3	250 psi	24 (9.2)	5
4 h	450°C	He	20 psi						
5 min	−196°C	He	20 psi	15.9	22.4	4.9	250 psi	24 (9.2)	6
12 h	450°C	He	20 psi						
5 min	−196°C	He	20 psi	18.7	28.7	4.6	250 psi	24 (9.2)	7
1 h	23 °C	H_2	20 psi	57.7	---	5.5	250 psi	24 (9.2)	8

Table 14. Activity of Ru/SiO_2; $Ru(NO)(NO_3)_3$ Precursor

Activation Conditions						Test Conditions			
Time	Temp	Gas	Pressure	β^s	β^m	β'	Pressure	CB–II–#(Wt%)	Trial
4 h	450 °C	H_2	20 psi	>100	---	4.5	200 psi	25 (1.15)	1
12 h	335 °C	He	20 psi	>100	---	6.0	200 psi	25 (1.15)	2
4 h	450 °C	H_2	20 psi	>100	---	4.5	200 psi	27 (3.9)	3
12 h	335 °C	He	20 psi	>100	---	6.3	200 psi	27 (3.9)	4
12 h	450 °C	H_2	20 psi						
2 h	450 °C	He	20 psi						
5 min	-196 °C	He	20 psi	33.7	40.4	5.5	250 psi	27 (3.9)	5
4 h	450 °C	He	20 psi						
5 min	-196 °C	He	20 psi	44.6	---	6.5	250 psi	27 (3.9)	6
4 h	450 °C	H_2	20 psi	>100	---	5.0	200 psi	29 (8.7)	7
12 h	450 °C	H_2	20 psi	>100	---	4.8	200 psi	29 (8.7)	8
12 h	335 °C	H_2	20 psi						
12 h	335 °C	He	20 psi						
5 min	-196 °C	He	20 psi	30.0	35.1	4.3	250 psi	29 (8.7)	9

Table 15. Activity of 8% Ru/SiO_2 with Pt Co-catalyst

Activation Conditions						Test Conditions			
Time	Temp	Gas	Pressure	β^s	β^m	β'	Pressure	CB–II–#	Trial
5 h.	450 °C	H_2	20 psi	40.8	---	4.0	200 psi	CB–II–44	1
12 h.	450 °C	H_2	20 psi	37.5	---	3.6	200 psi	CB–II–44	2
5 h.	450 °C	H_2	20 psi	42.0	---	3.6	200 psi	CB–II–45	3
12 h.	450 °C	H_2	20 psi	42.0	---	3.7	200 psi	CB–II–45	4

Table 16. Activity of Catalysts Prepared by Alternative Methods

Activation Conditions				Test Conditions					
Time	Temp	Gas	Pressure	β^s	β^m	β'	Pressure	CB–II–#	Trial
4 h.	335 °C	H_2	20 psi	>100	---	4.0	200 psi	CB–II–37	1
4 h.	450 °C	H_2	20 psi	74	---	3.2	200 psi	CB–II–37	2
12 h.	450 °C	H_2	20 psi	58	---	3.3	200 psi	CB–II–37	3
8 h.	450 °C	H_2	20 psi						
12 h.	450 °C	He	20 psi						
5 min.	-196°C	He	20 psi	15.8	19.9	6.3	200 psi	CB–II–37	4
4 h.	450 °C	H_2	20 psi	74	---	3.2	200 psi	CB–II–48W	5
8 h.	450 °C	H_2	20 psi						
12 h.	450 °C	He	20 psi						
5 min.	-196°C	He	20 psi	34.7	---	5.3	200 psi	CB–II–48W	6

Table 17. Activity of Ru Ammine Catalysts; $Ru(NO)(NO_3)_3$ Precursor

Catalyst	Ru Weight %	β^s [H_2]	β^s [H_2–He]
CB–II–106	2.03	20.3	14.3
CB–II–105	3.91	9.0	6.8
CB–II–88	6.61	5.9	4.3
CB–II–92	8.47	6.9	4.0
CB–II–117	10.15	8.5	5.0

Table 18. Activity of Chloride Containing Ruthenium Precursor–Activity of Alternative Catalyst Preparations

Catalyst	Precursor	Ru Weight %	β^s [H_2]	β^s [H_2–He]
CB–II–89	$RuCl_3$	7.33	>125	41.7
CB–II–93	$Ru(NO)Cl_3$	7.02	83.3	60.6
CB–II–89W	$RuCl_3$	7.33	>125	45.3
CB–II–125	$Ru(NO)(NO_3)_3$	7.20	8.5	5.6
CB–II–130	$RuCl_3$	5.55	9.6	4.5

Table 19. Results of (η^4–cyclohexa–1,3–diene)(η^6–benzene) Ruthenium Precursor Catalysts

Metal Loading	Activating Gas	β'	Temp (β')	β^s
3.5	H_2	2.28	- 145°C	67.67
4.0	H_2	2.36	- 149°C	84.34
	He	2.43	- 149°C	57.07
4.7	H_2	2.31	- 160°C	25.62
	He	3.21	- 172°C	20.4
6.0	H_2	2.24	- 156°C	18.11
	He	2.62	- 160°C	21.93
14.0	H_2	3.09	- 170°C	11.55
	He	2.21	- 166°C	10.94
17.2	H_2	1.85	- 173°C	10.54
	He	2.16	- 176°C	8.88
23.7	H_2	1.81	- 168°C	11.31
	He	2.03	- 172°C	7.35

Table 20. Dispersion of Ruthenium Ammine Precursor Catalysts Prepared with $Ru(NO)(NO_3)_3$

Catalyst	Metal Content	Dispersion	Ru Atoms/Gram ($x10^{19}$)
CB–II–106	2.03 %	39.4 %	4.69
CB–II–105	3.91 %	24.5 %	5.84
CB–II–88	6.61 %	32.7 %	12.96
CB–II–92	8.47 %	19.38 %	9.78
CB–II–117	10.15 %	9.0 %	5.43
CB–II–125	7.20 %	34.22 %	14.32

Table 21. Dispersion of Ammine Precursor Catalyst Prepared by Alternative Procedures

Catalyst	Precursor	Metal Content	Dispersion	Ru Atoms/Gram ($x10^{19}$)
CB–II–89	$RuCl_3$	7.33 %	3.40 %	1.49
CB–II–93	$Ru(NO)Cl_3$	7.02 %	13.32 %	5.57
CB–II–89W	$RuCl_3$	7.33 %	3.38 %	1.48
CB–II–130	$RuCl_3$	5.55 %	37.75 %	12.37

Table 22. Dispersions of Selected Traditional Ruthenium Catalysts

Catalyst	Precursor	Metal Content	Dispersion	Ru Atoms/Gram ($x10^{19}$)
CB–II–19	$RuCl_3$	4.37 %	11.9 %	3.10
CB–II–23	$Ru(NO)Cl_3$	5.86 %	6.23 %	2.18
CB–II–27	$Ru(NO)(NO_3)_3$	3.94 %	1.8 %	0.461

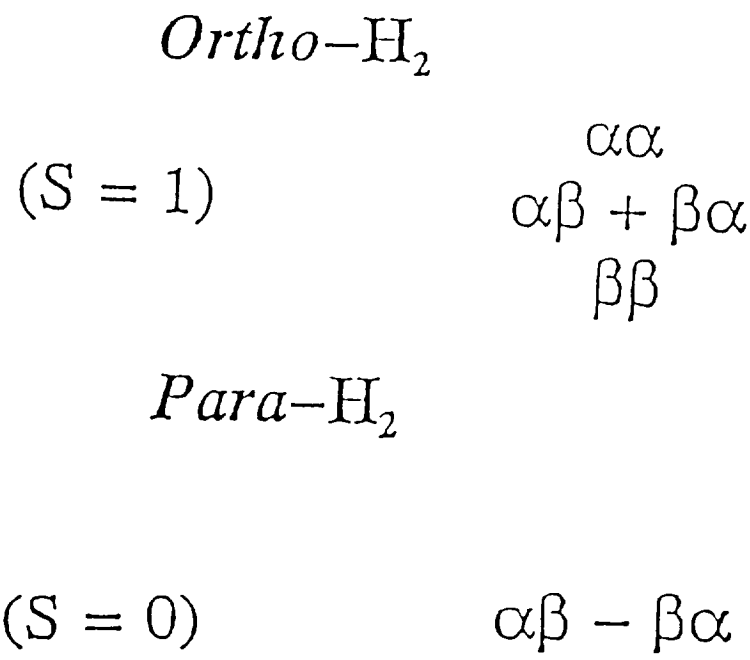

Figure 1. Schematic of the Degeneracy of the Two Forms of Hydrogen

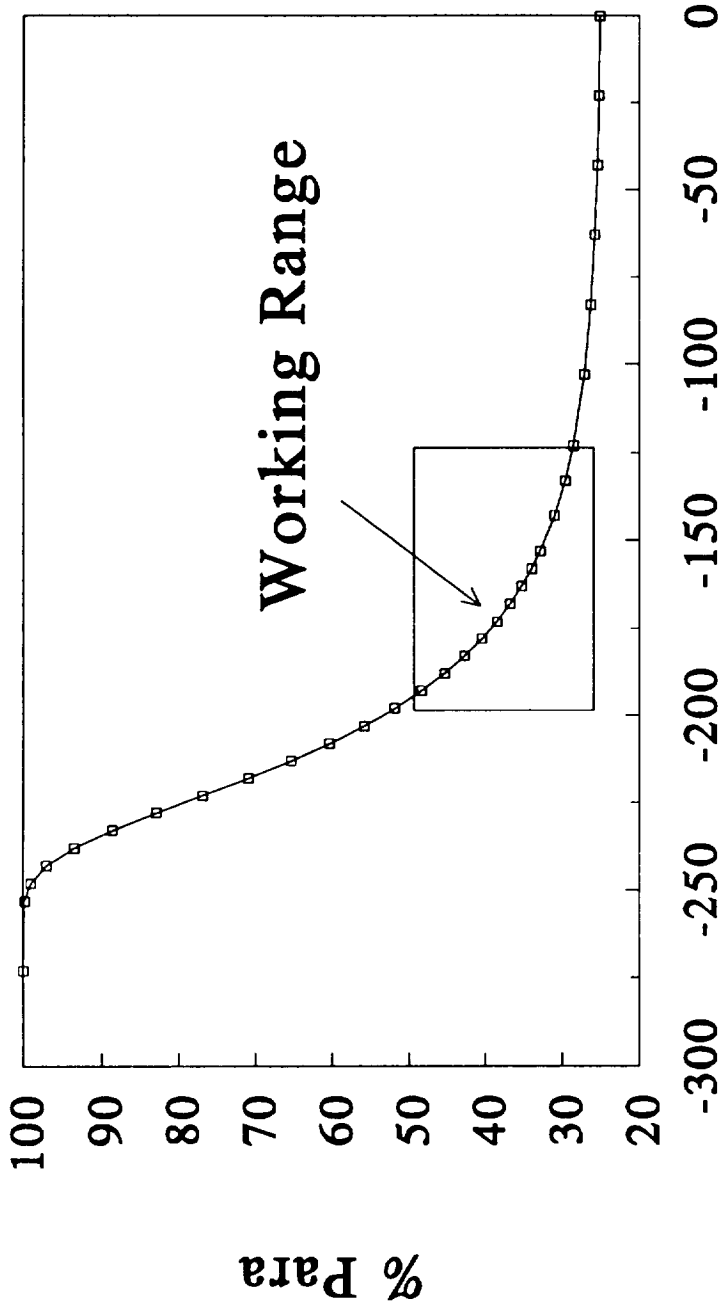

Figure 2. Equilibrium Composition of *ortho*- and *para*-Hydrogen vs. Temperature

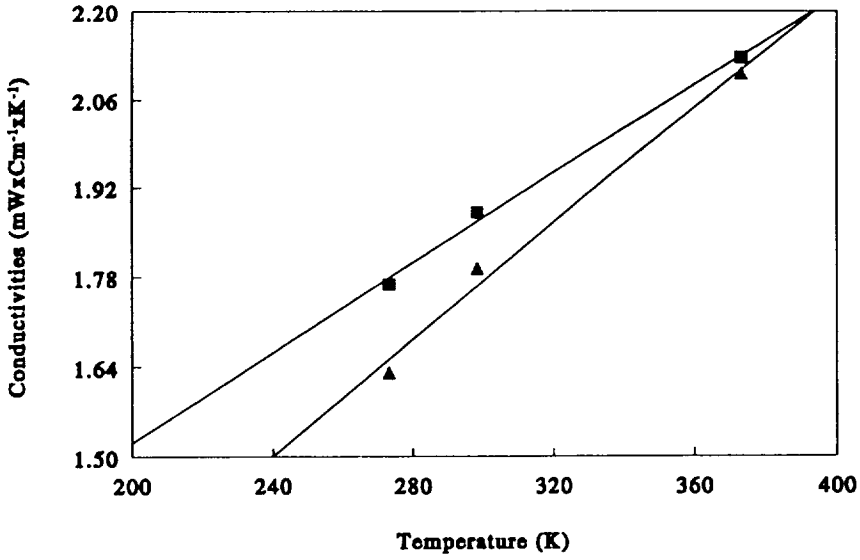

Figure 3. Thermal Conductivities of H_2vs. Temperature (▲ *ortho-* ■ *para-*

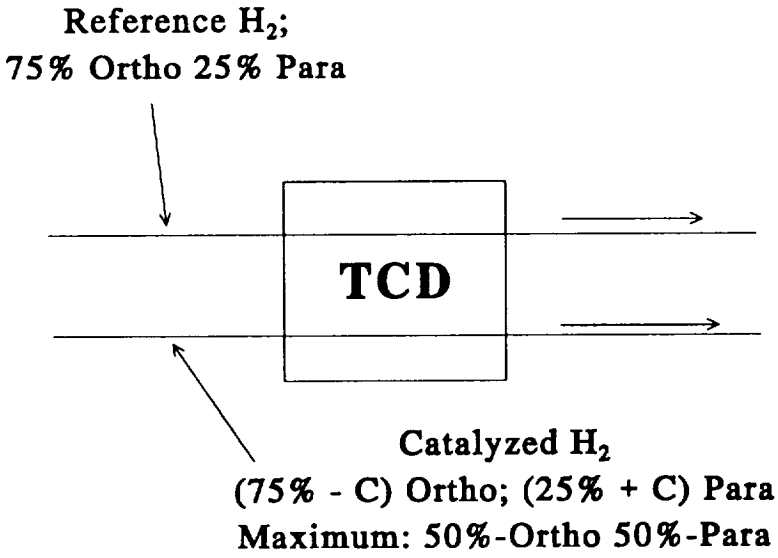

Figure 4. Simplified Schematic for Detection of *ortho-* and *para-*H_2Compositions.

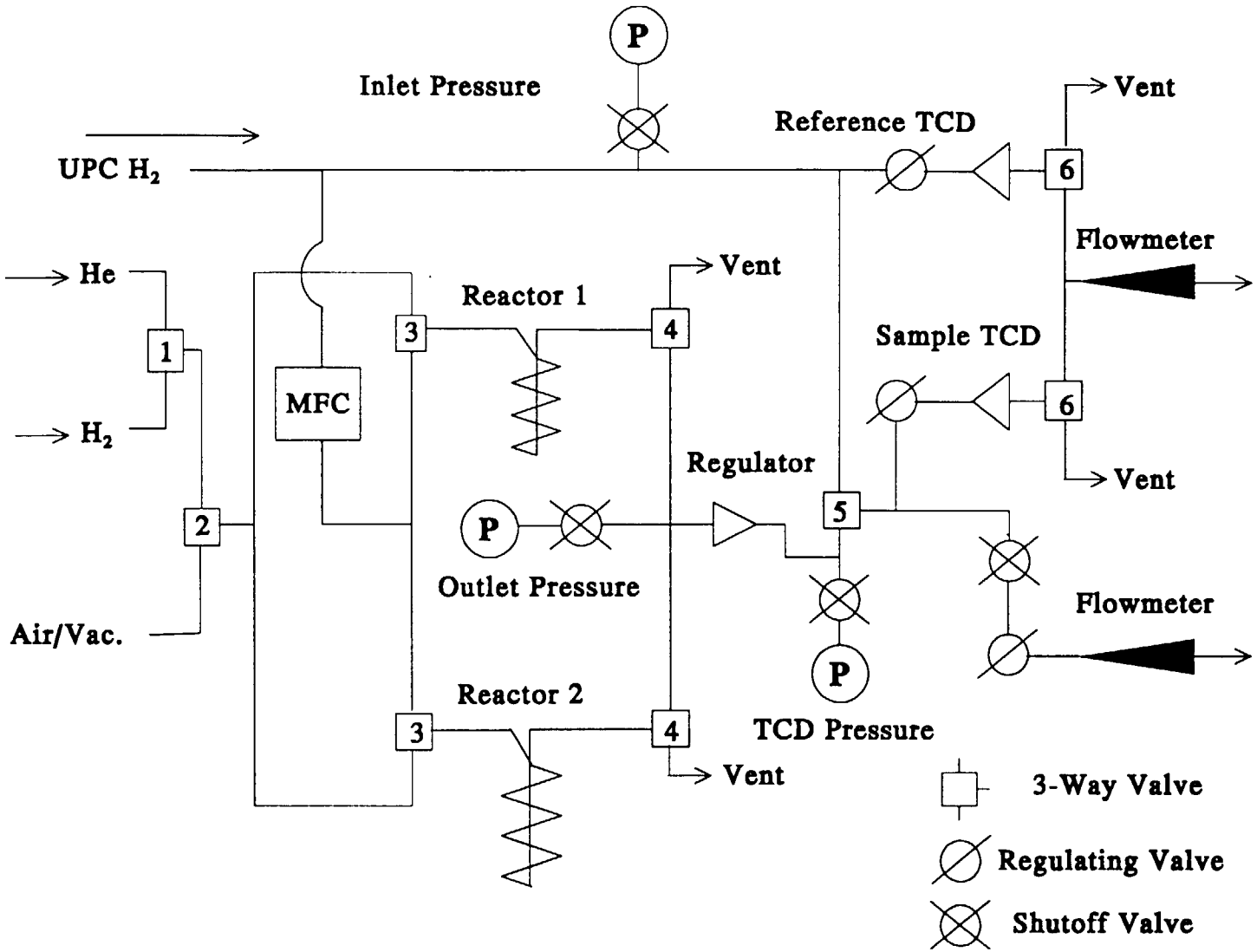

Figure 5. Reactor Schematic for Catalytic Conversion of *ortho-* to *para*-H_2

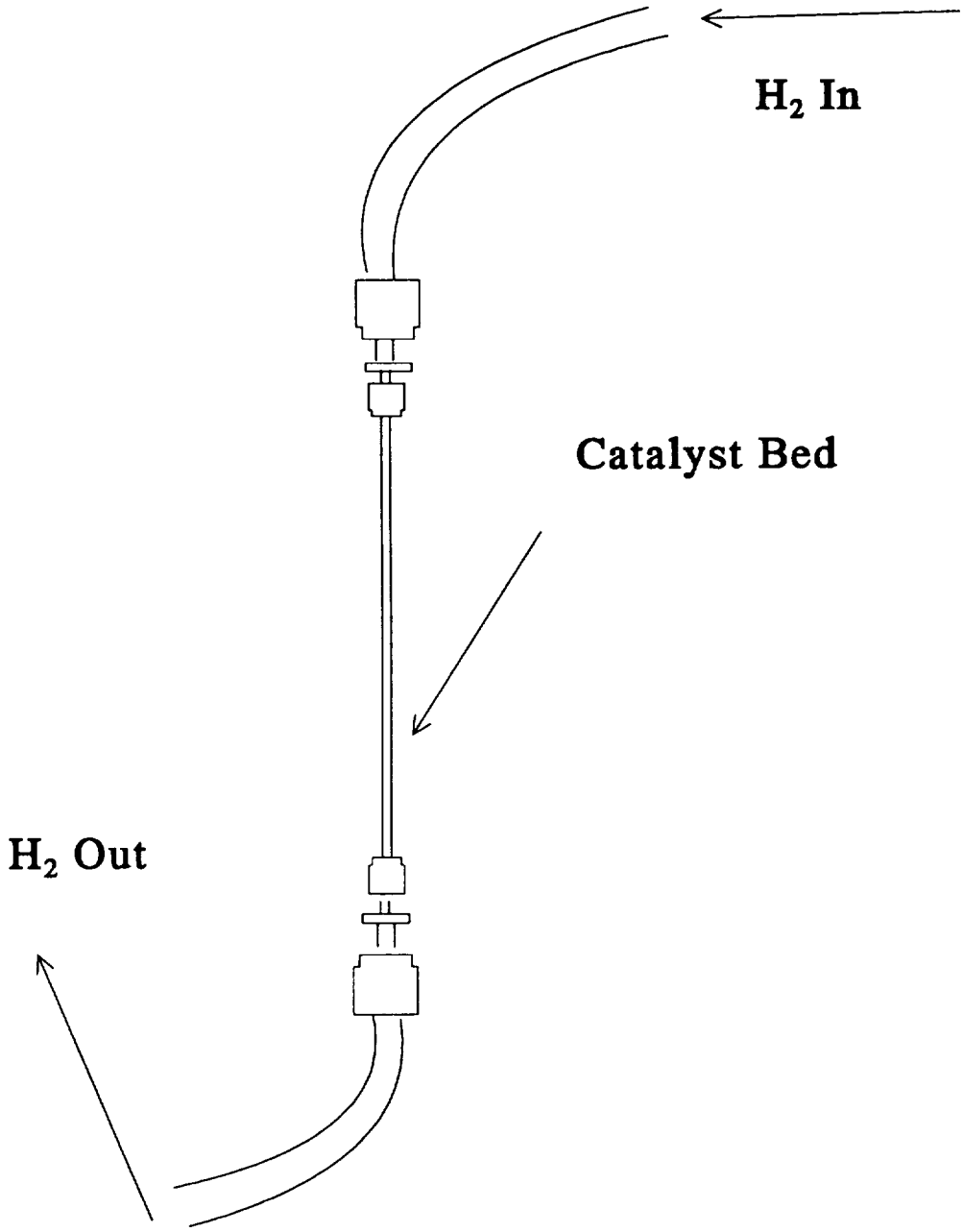

Figure 6. Reactor Tube Assembly 1; Without Thermocouple

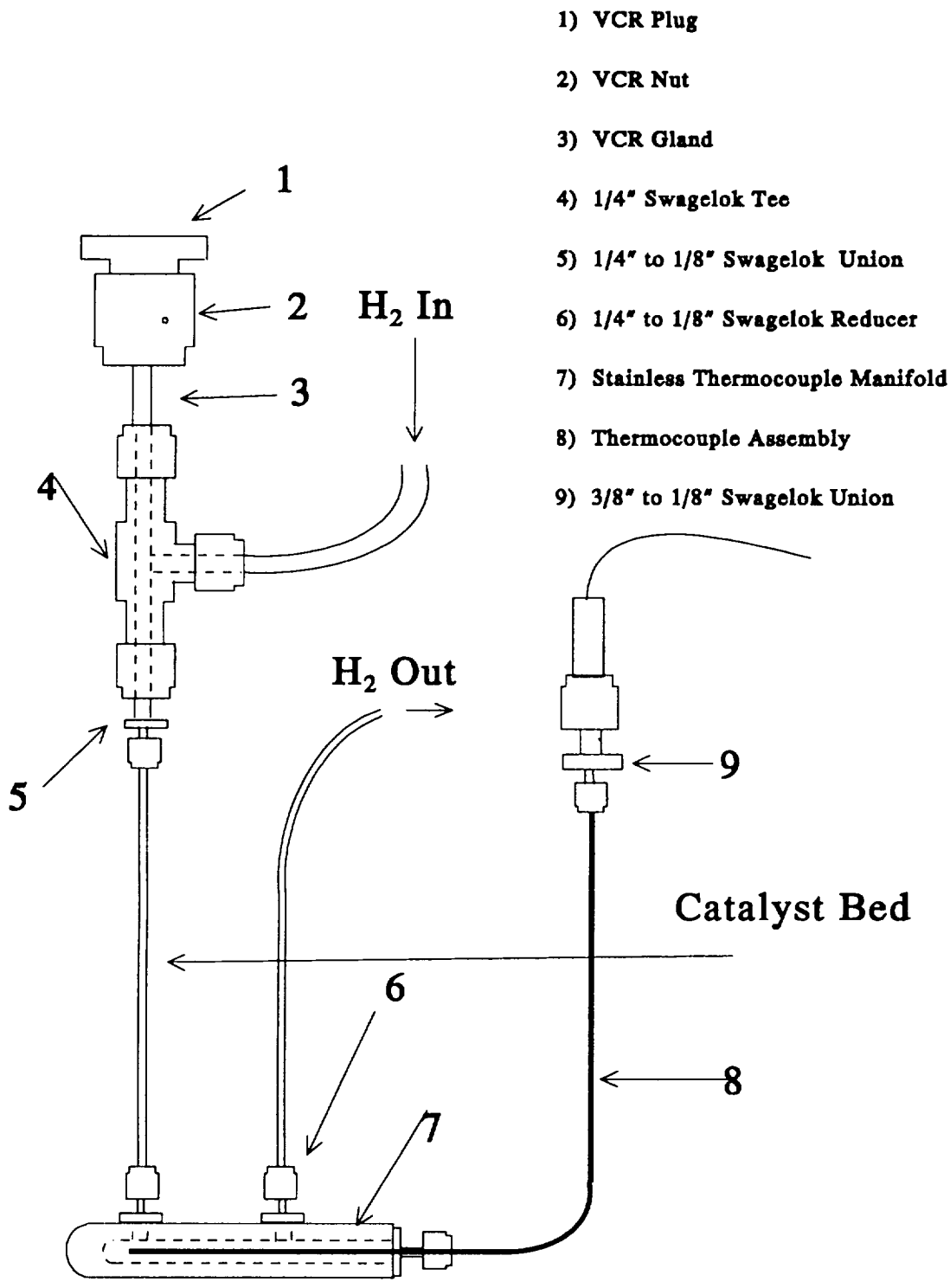

Figure 7. Reactor Tube Assembly 2; Bent Thermocouple

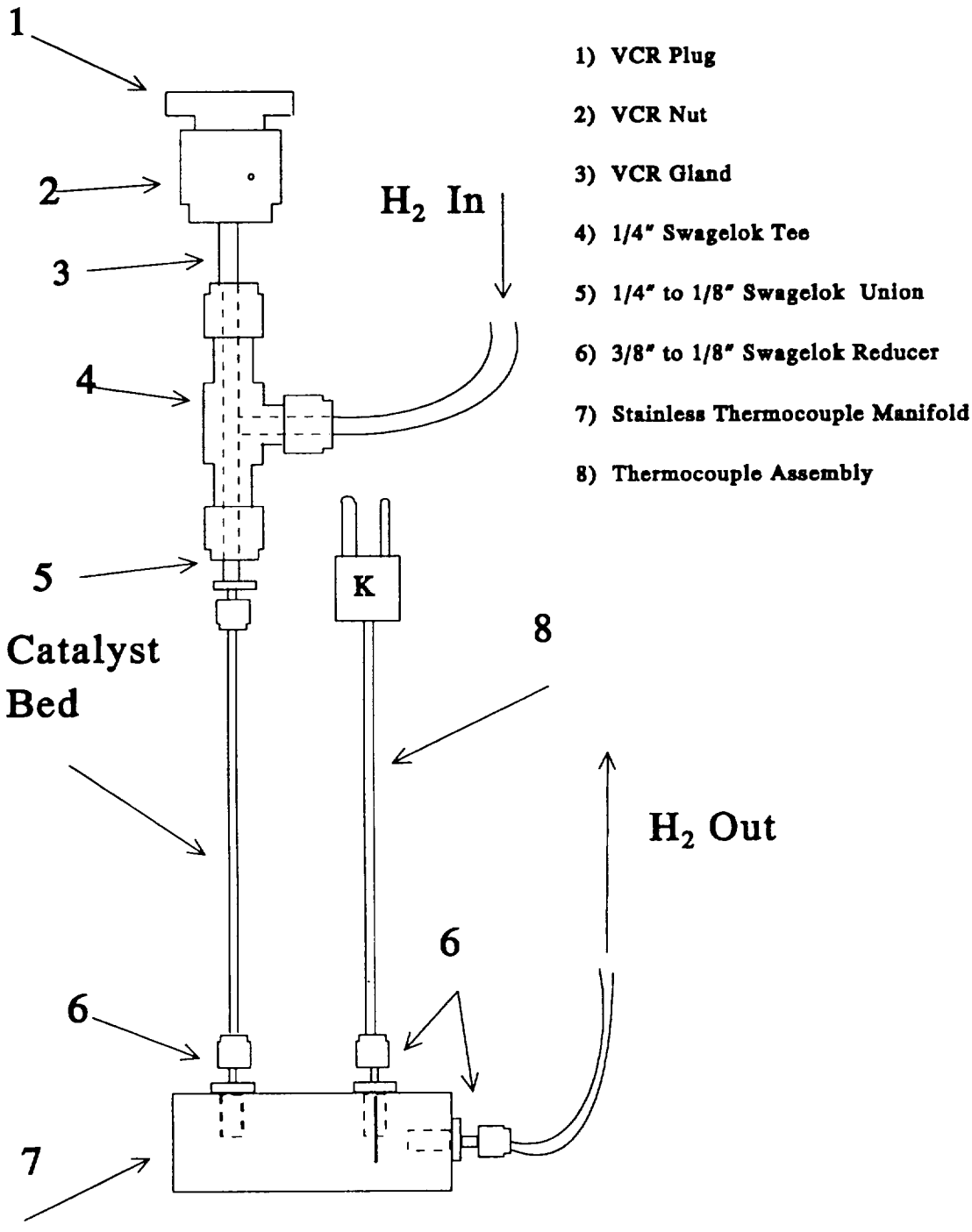

Figure 8. Reactor Tube Assembly 3; Straight Thermocouple

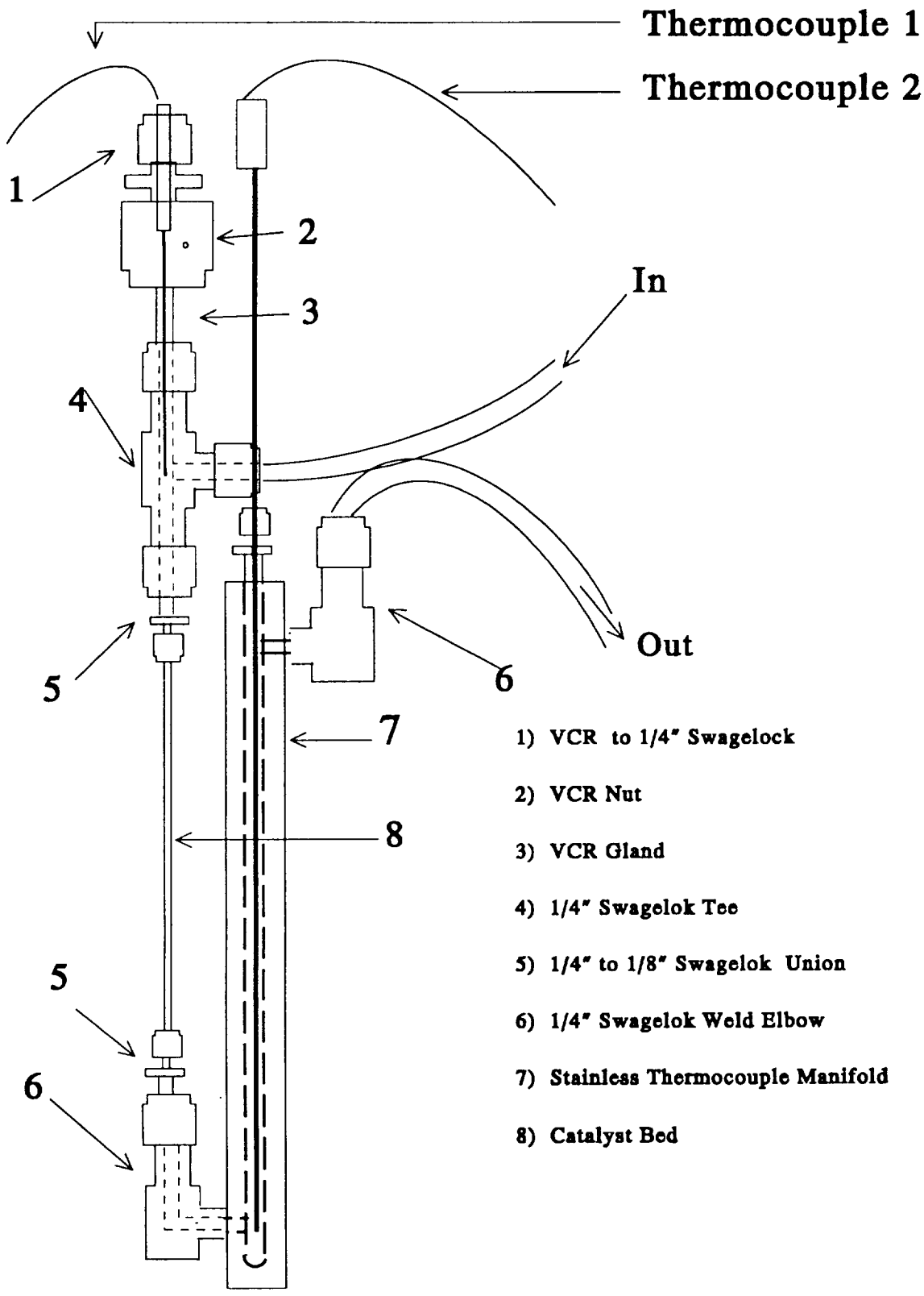

Figure 9. Reactor Tube Assembly 4; 2 Thermocouples

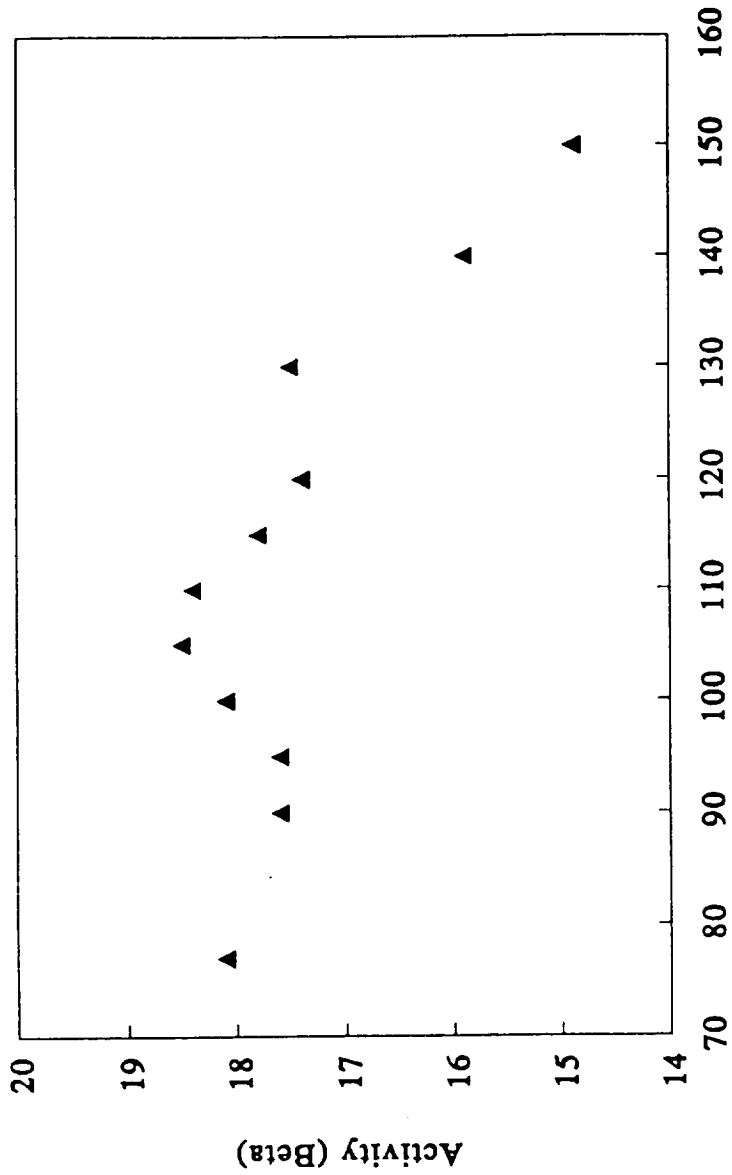

Figure 10. Activity of Nickel Silicate (AP) vs. Temperature

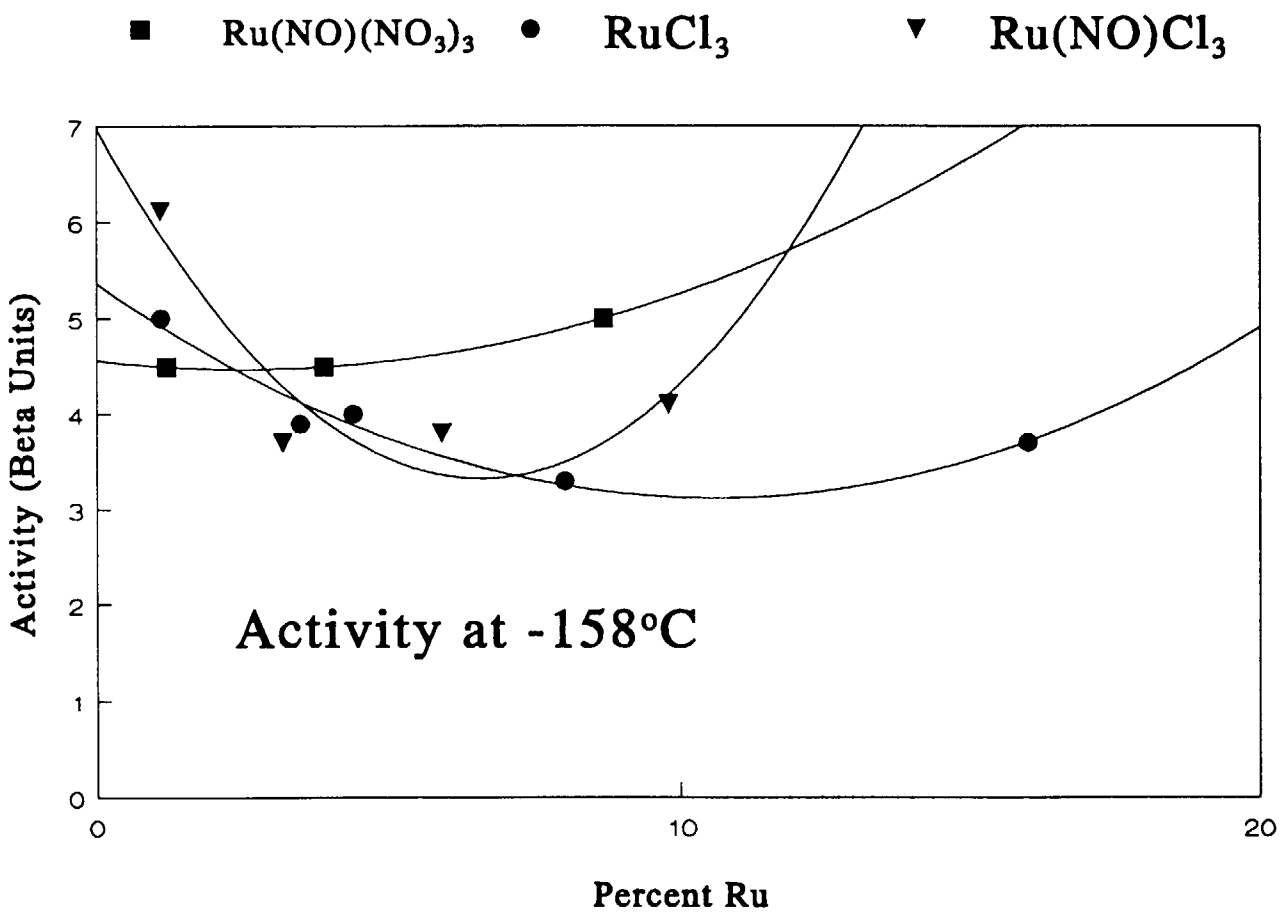

Figure 11. Activity of Ruthenium Catalysts at -158 °C as a Function of Ru Precursor

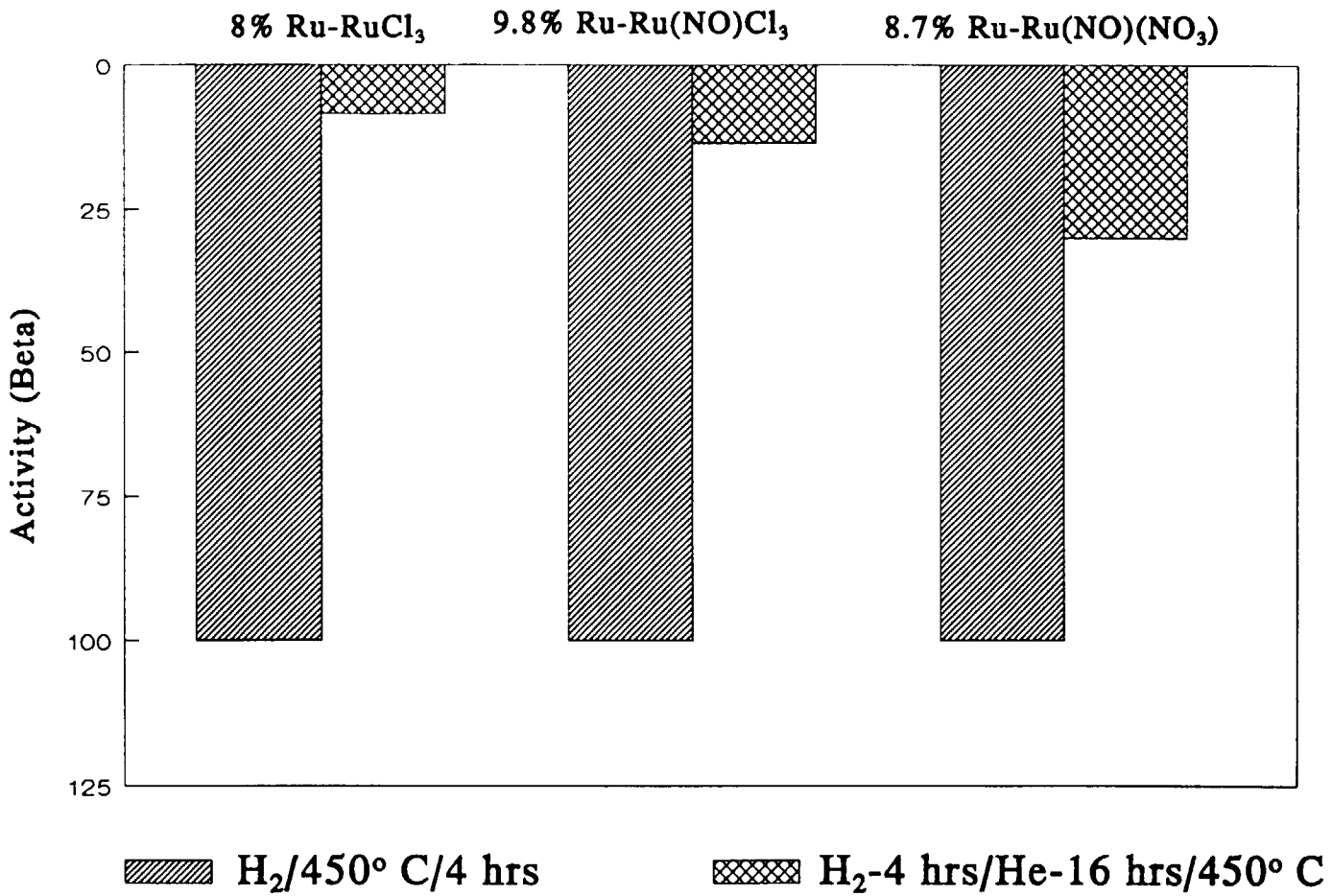

Figure 12. Effect of Ruthenium Precursor on "He Effect" Activity at -196 °C

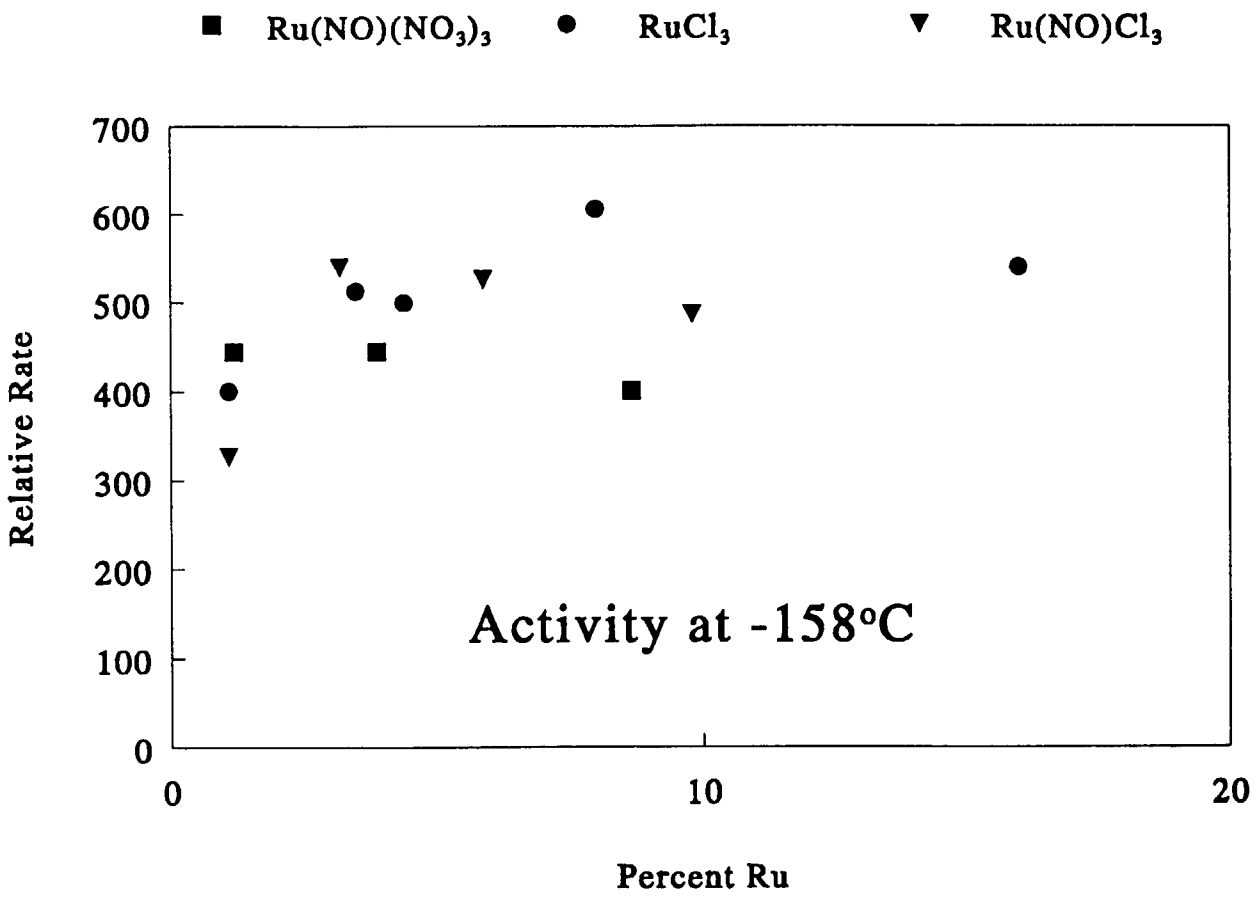

Figure 13. Activity of Ruthenium Ammine Catalysts; $Ru(NO)(NO_3)_3$ Precursor as a Function of % Ruthenium Loading

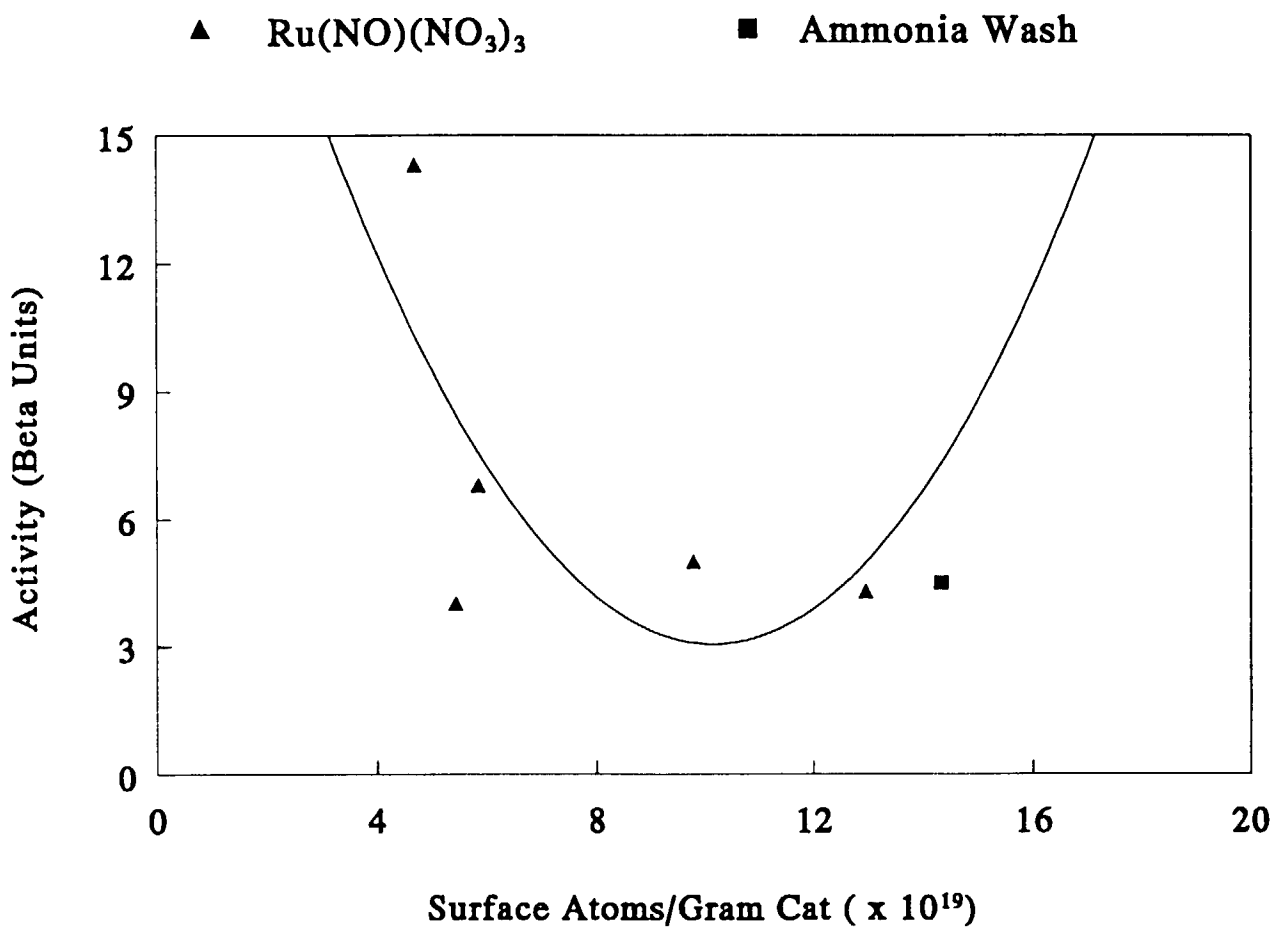

Figure 14. "He Effect" β values vs. Surface Ru Atoms/Gram Catalyst

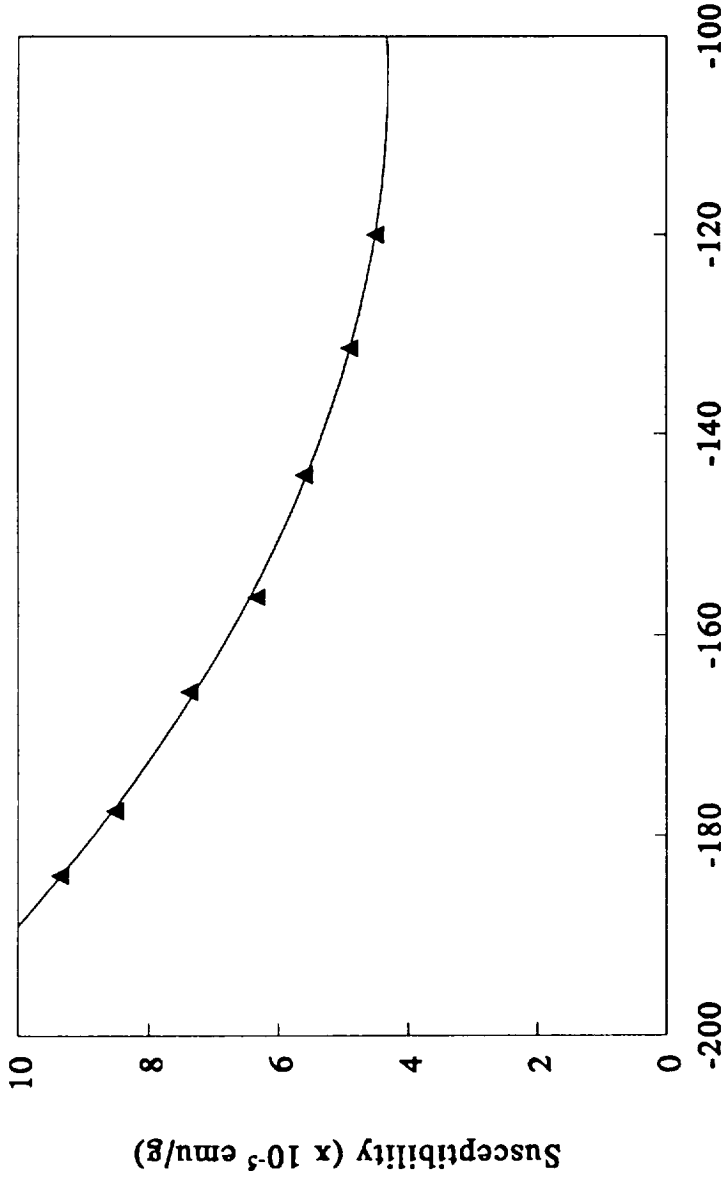

Figure 15. Magnetic Susceptibility of Activated Air Products vs. Temperature

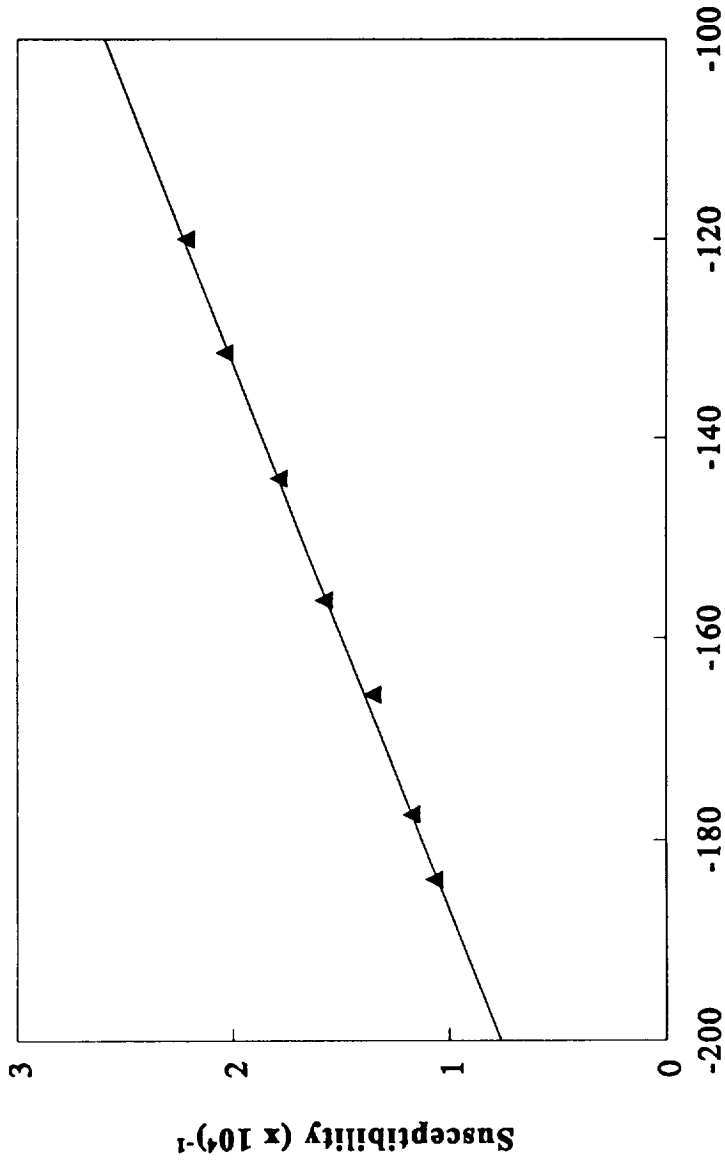

Figure 16. Inverse Susceptibility vs. Temperature

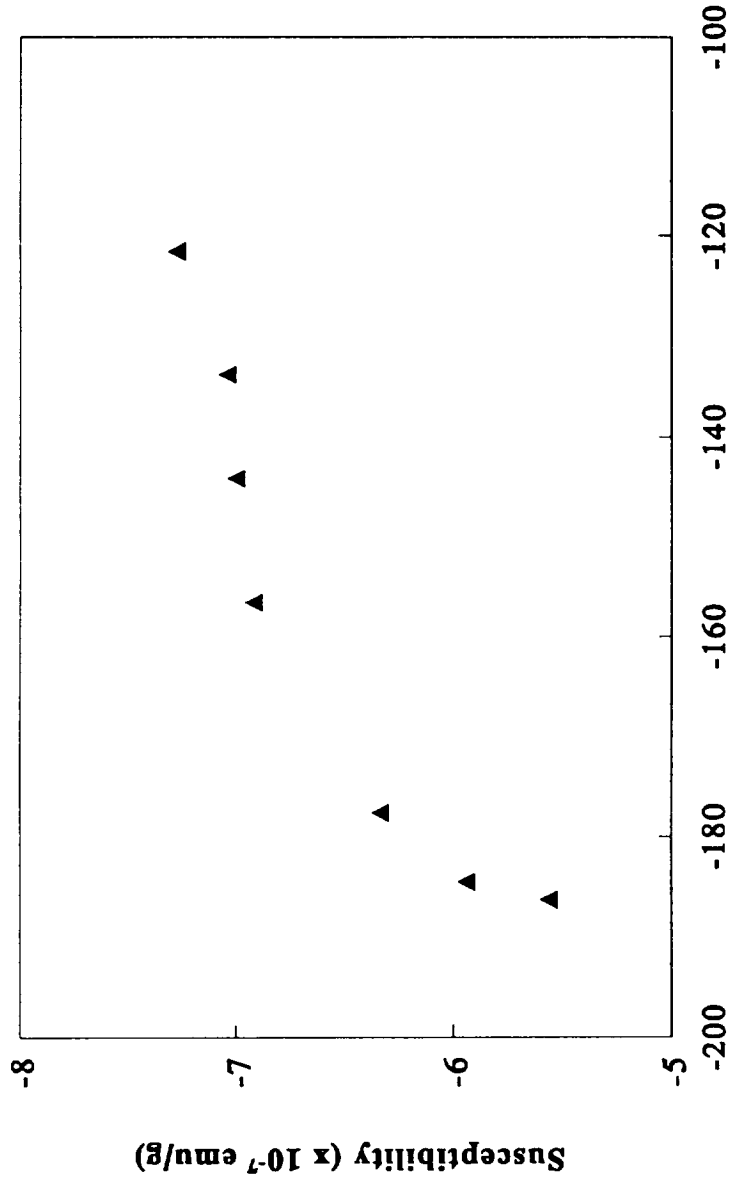

Figure 17. Magnetic Susceptibility of CB–II–24 vs. Temperature; No Activation

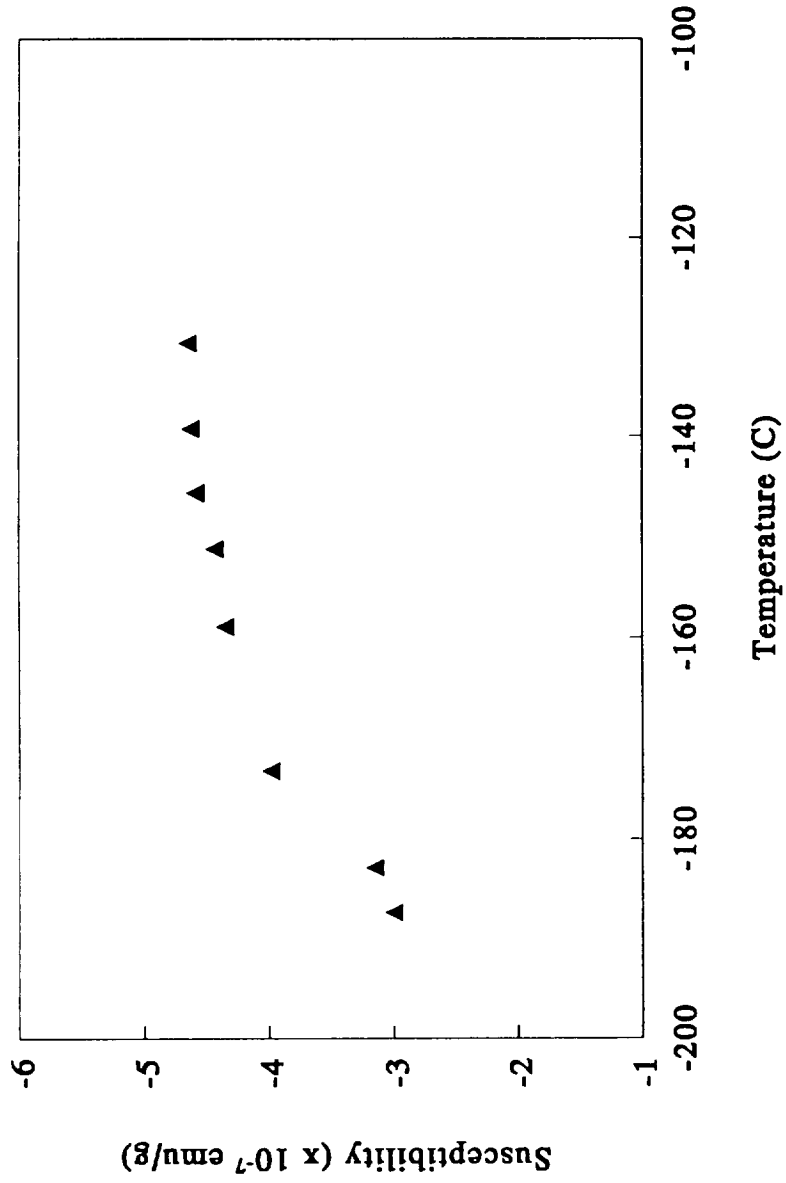

Figure 18. Magnetic Susceptibility of CB–II–24 vs. Temperature; Reduced in H_2 at 350 °C

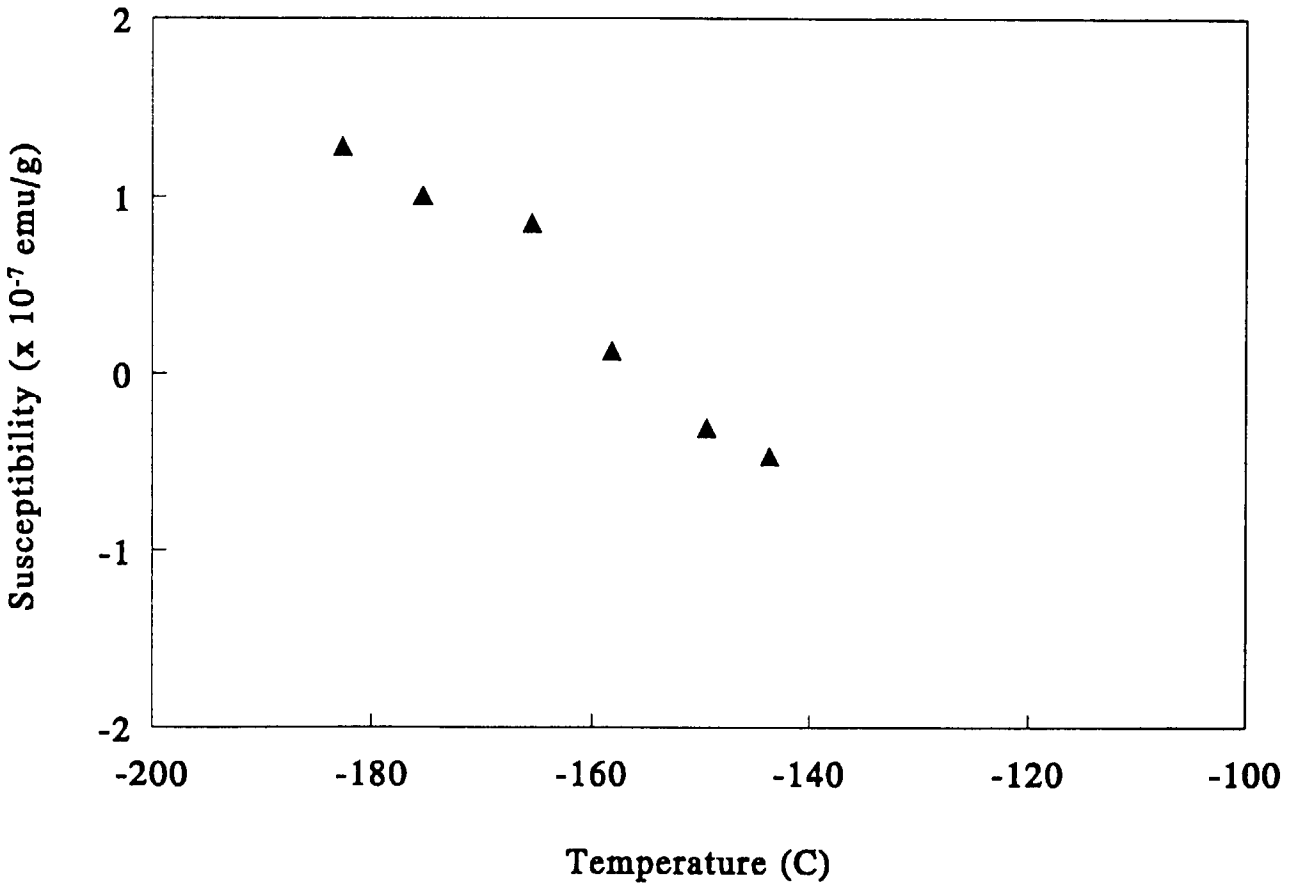

Figure 19. Magnetic Susceptibility of BF–40Cl vs. Temperature; Reduced in H_2 at 350 °C

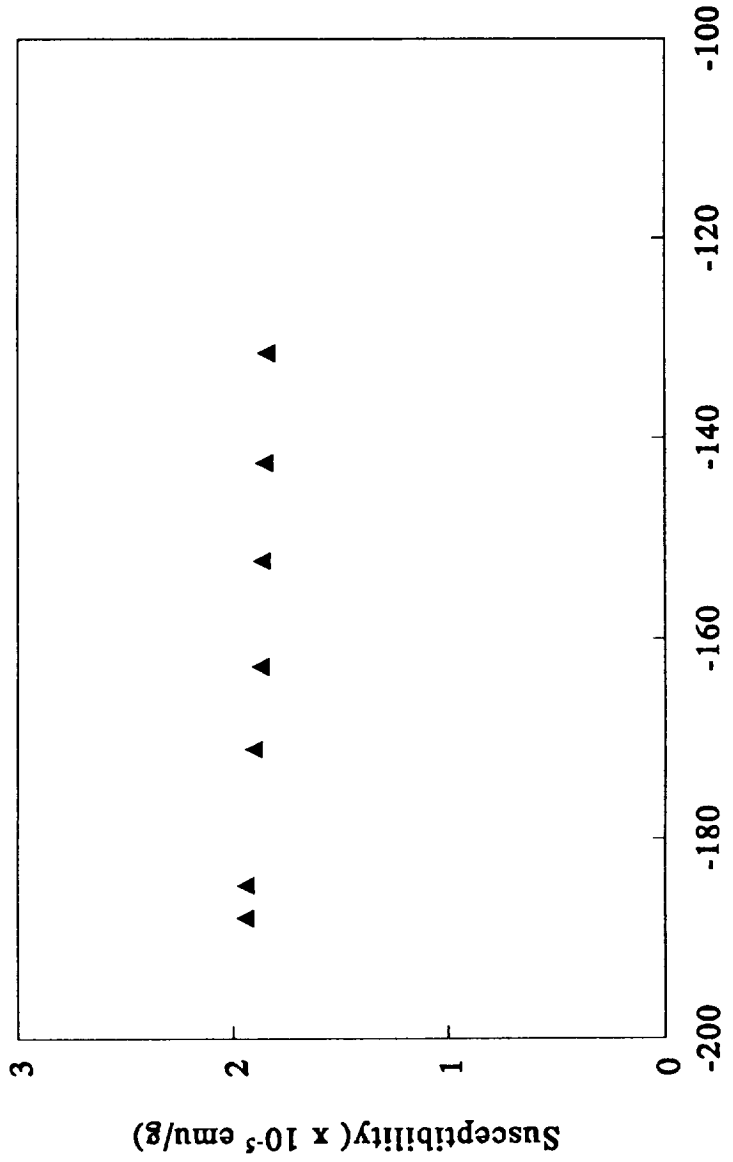

Figure 20. Magnetic Susceptibility of WW–17 vs. Temperature; No Activation

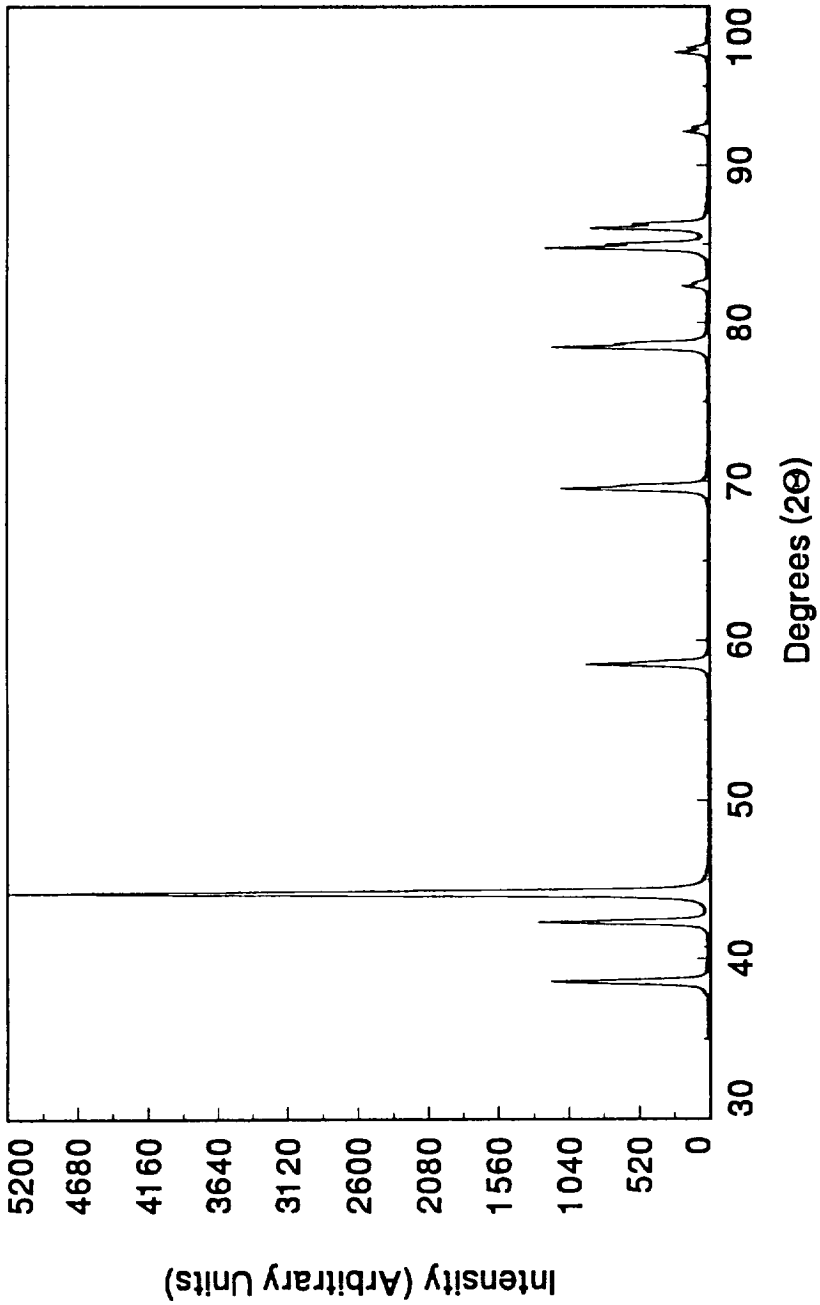

Figure 21. XRD of Ruthenium Metal

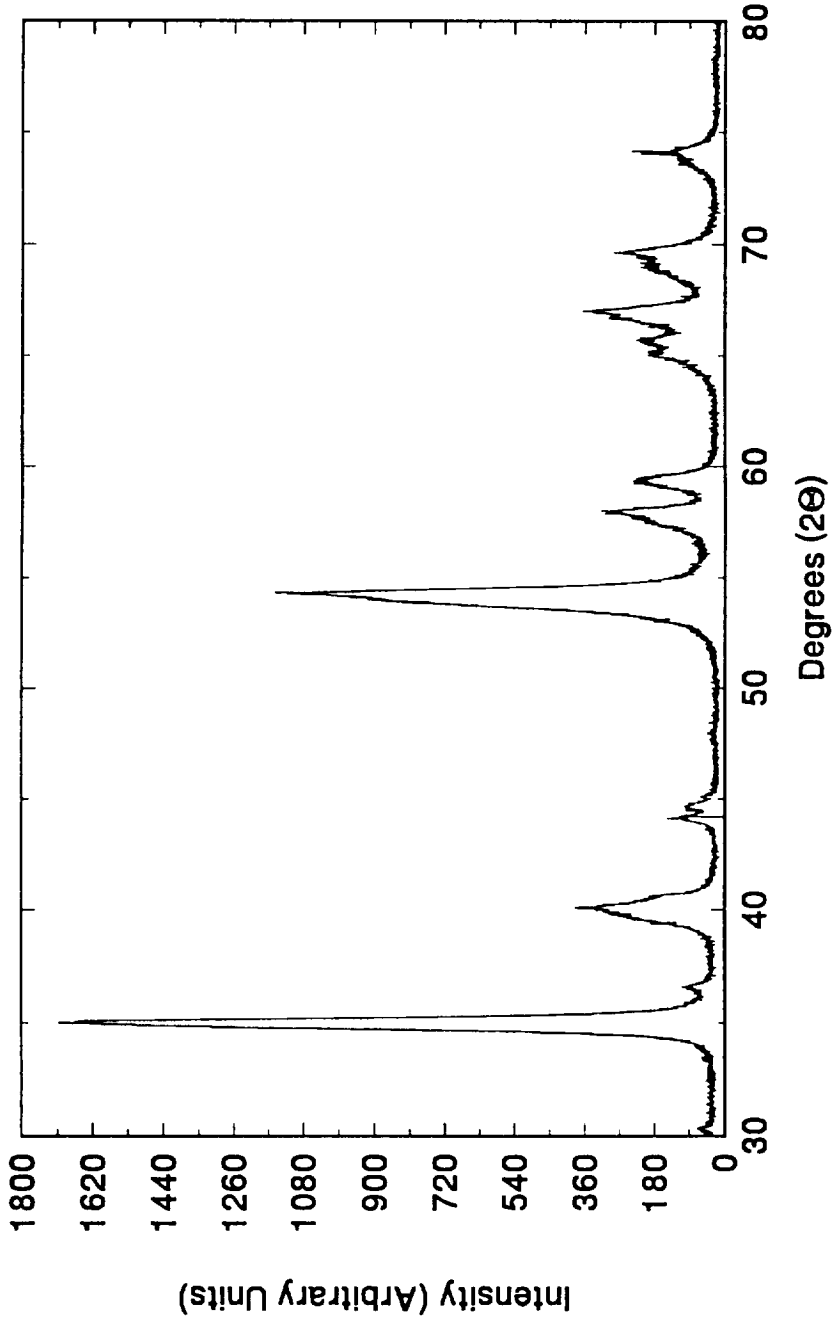

Figure 22. XRD of RuO_2

C-2

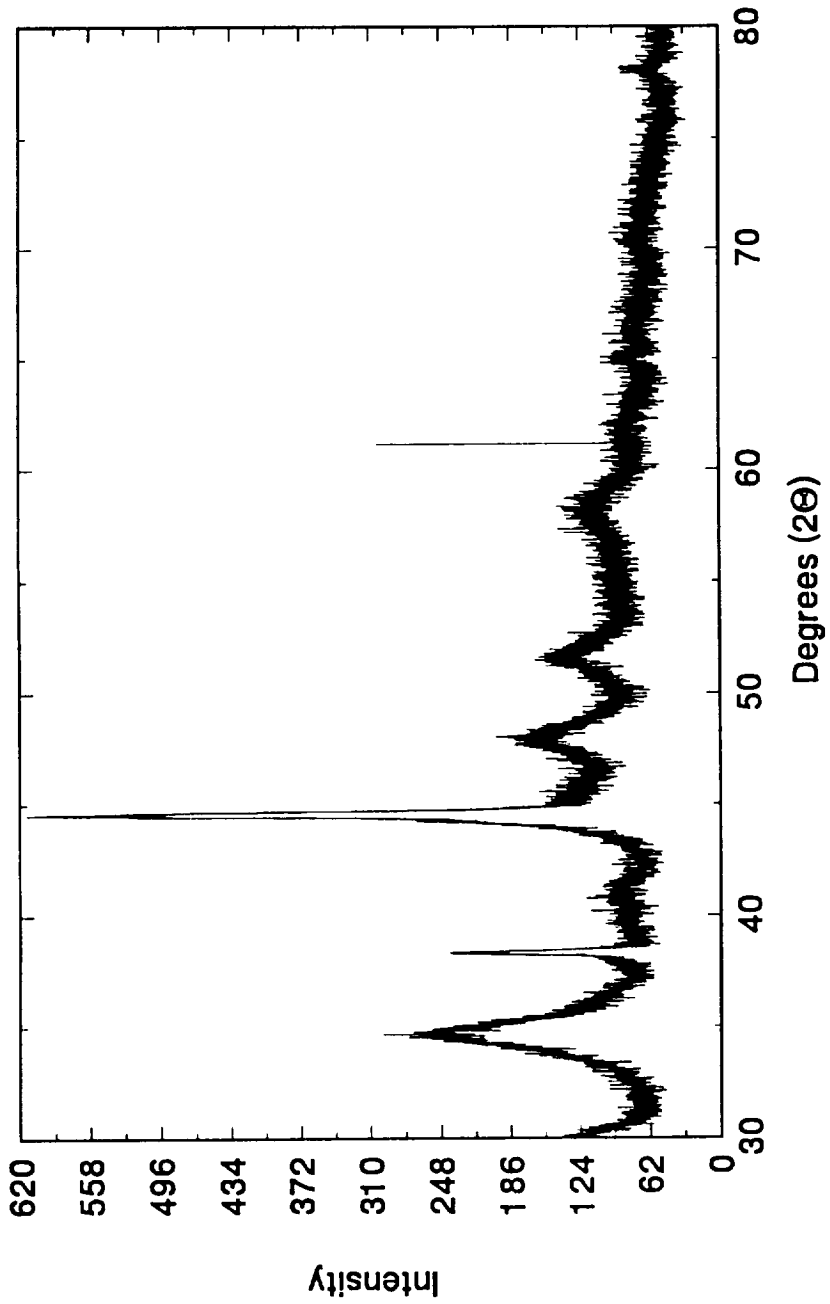

Figure 23. XRD of $RuCl_3$

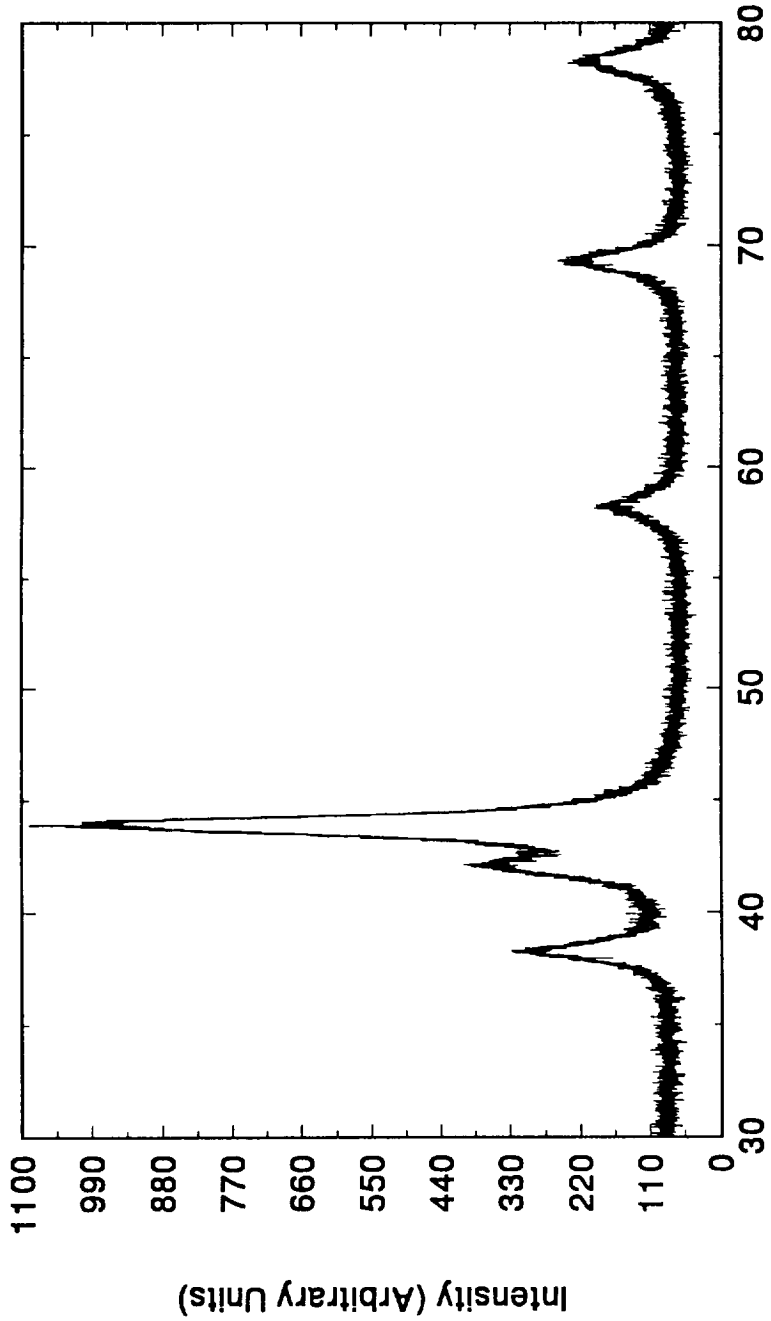

Figure 24. XRD of CB–II–46; 16% Ruthenium on Silica

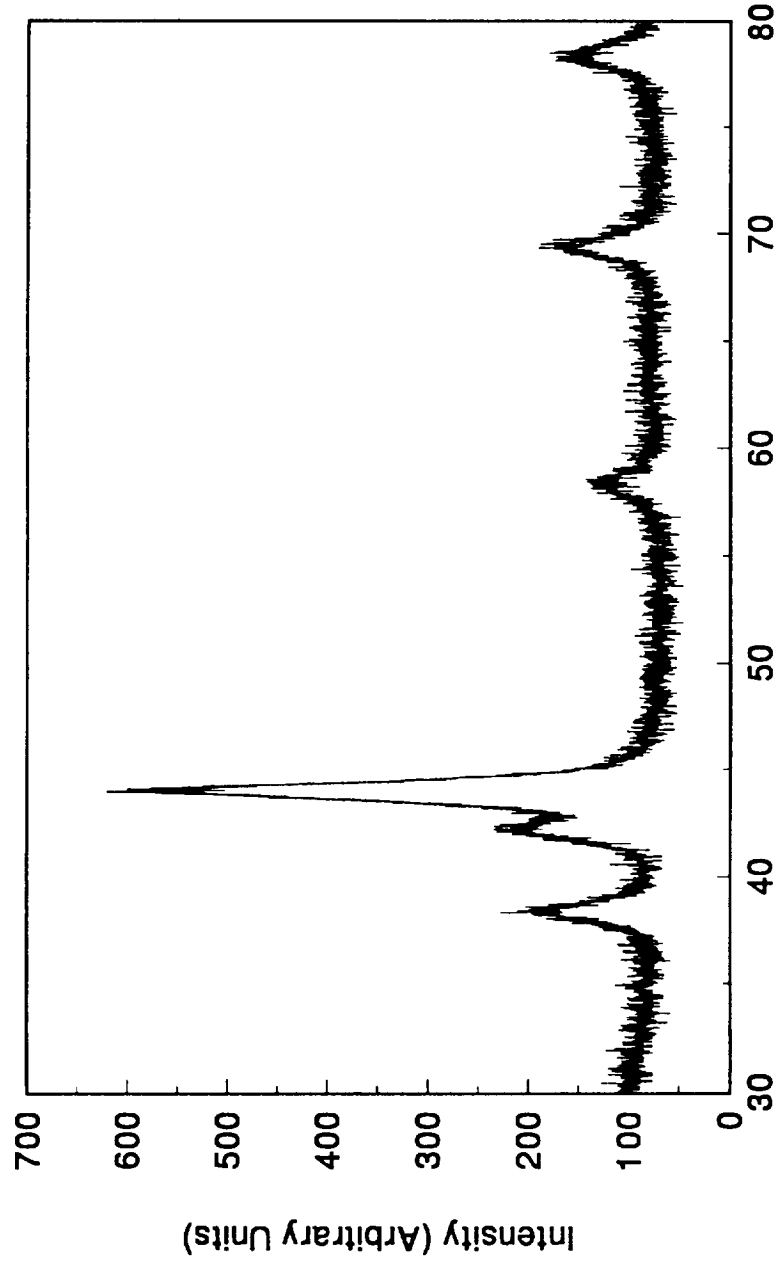

Figure 25. XRD of CB–II–48; 8% Ruthenium on Silica

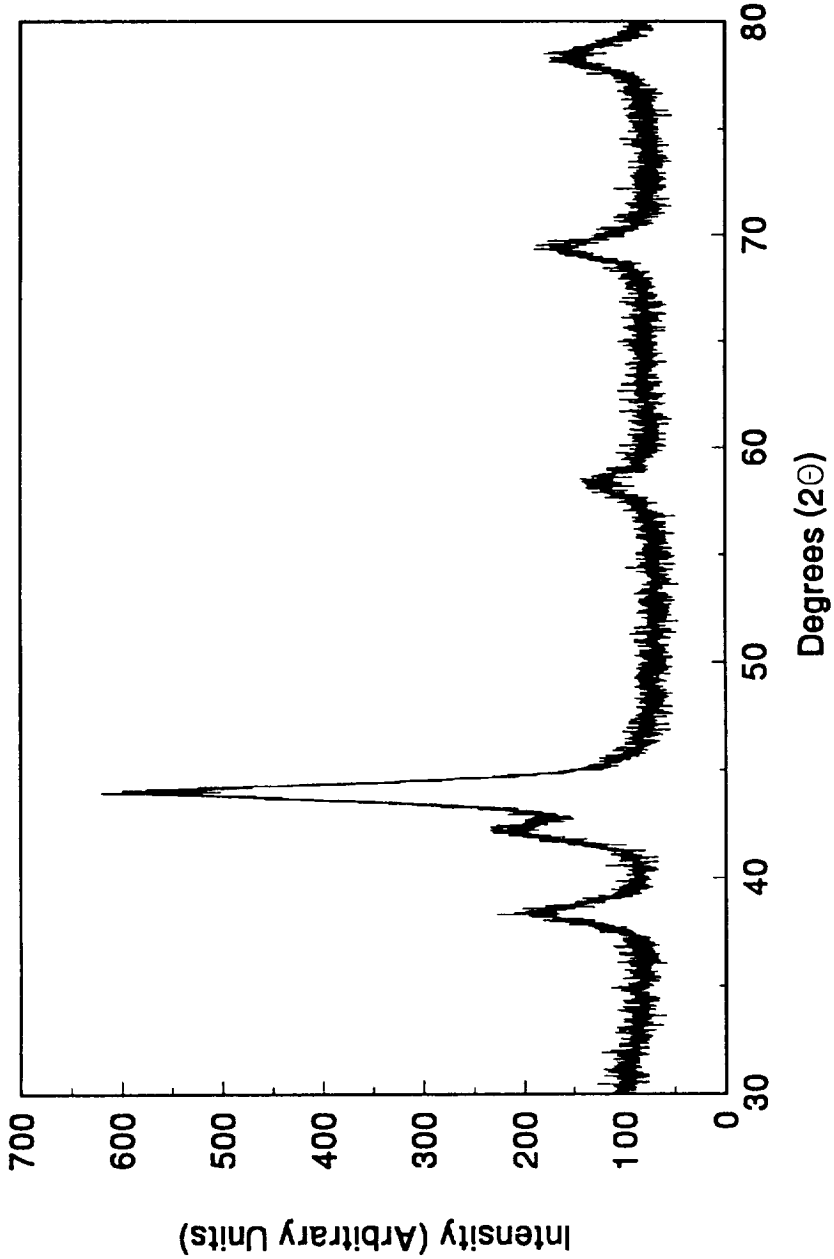

Figure 26. XRD of CB–II–48W; Hot Water Wash

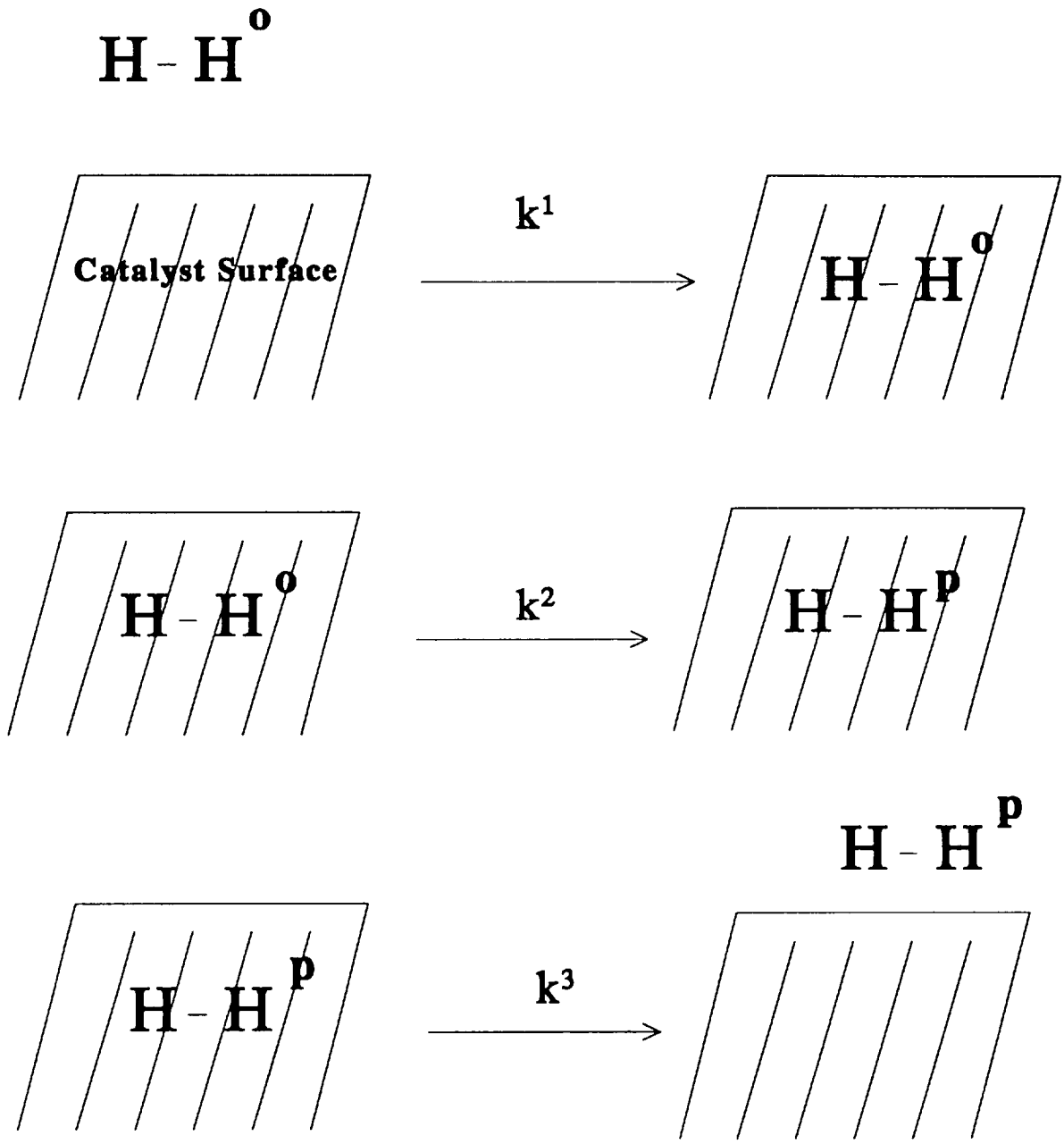

Figure 27. Physical Process for *ortho-* to *para*-H_2 Conversion

a) Ru Catalyst / No Cl Present

Surface
Cooled in H_2

Surface
Purged/Cooled in He

b) Ru Catalyst / Cl Precursor

Surface
Cooled in H_2

Surface
Purged/Cooled in He

Figure 28. Schematic of Proposed Surface Following H_2 Activation and He Purge

REFERENCES

(1) Barron, R. *Cryogenic Systems*; Oxford University; New York, 1985, p 47.

(2) *Comprehensive Inorganic Chemistry*, Perganon; New York; 1973, Vol. I, p 11.

(3) Noggle, J. H. *Physical Chemistry* Little, Brown and Company, Boston.

(4) Farkus, L., and Sachsee, H. *Z. Physik. Chem*, **1933**, B23, 19.

(5) Wigner, E. *Z. Physik. Chem.*, **1933**, B23, 28.

(6) Petzinger, K. G., and Scalapino, D. J. *Physical Review B*, **1973**, 8, 266.

(7) Coffman, R. E. "Final Technical Report to NASA", 1992.

(8) Stevenson, R. *J. Catal.* **1983**, 79, 218.

(9) Van Cauwelaert, F. H., and Hall, W. K., *Trans. Faraday Soc.*, **1970**, 66, 454.

(10) Scott, R. B., Brickwedde, F. G., Urey, H. C., and Wahl, M. H. *J. Chem. Phys.*, **1934**, 2, 454.

(11) Chapin, D. S., Cunningham, C. M., and Johnston, H. L. *Advances in Cryogenic Engineering*; Plenum, 1960; Vol. I, p 280.

(12) Arias, J.A., and Selwood, P.W. *J. Catal.* **1974**, 33, 284.

(13) Eley, D. D., Forrest, H., and Rudham, R. *J. Catal.*, **1974**, 34, 35.

(14) a) Selwood, P. W. *J. Catal.* **1970**, 19, 353.
b) Selwood, P. W. *J. Catal.* **1971**, 22, 123.
c) Madhusudhan, C. P,. and Selwood, P. W. *J. Catal.*, **1976**, 45, 106.

(15) Rudham, R., Tullett, A. D., and Wagstaff, K. P. *J. Catal.*, **1975**, 38, 488.

(16) Singleton, A. H., Lapin, A., and Wenzel, L. A. *Advances in Cryogenic Engineering*; Timmerhaus, K. D. Ed.; Plenum: New York; 1968, Vol XIII, p 409.

(17) Barrick, P. L., Brown, L. F., Hutchinson, H. L., and Cruse, R. L. *Advances in Cryogenic Engineering*; Plenum: New York, 1965, Vol X, p 181.

(18) Haley, A. J., and Hinden, S. G. "Englehard Technical Report AFAPL–TR–65–59" (1965).

(19) Anderson, J. R.; Pratt, K. C. *Introduction to Characterization and Testing of Catalysts*, Academic, New York, 1985.

(20) a) *Modern Practices of Gas Chromatography*, Grob, R. L. Ed.; Wiley, New York, 1977.
b) Littlewood, A. B., *Gas Chromatography*, Academic, New York, 1970.

(21) Weitzel, D. H., and White, L. E. *Rev. Sci. Inst.*, **1955**, 23, 290.

(22) Barron, R. *Cryogenic Systems*; Oxford University; New York, 1985

(23) Barrick, P. L., Brown, L. F., Hutchinson, H. L., and Cruse, R. L. *Advances in Cryogenic Engineering*; Plenum: New York, 1965, Vol X, p 181.

(24) Nykerk, K. M., Eyman, D. P., Simth, R. L. *Inorganic Chemistry*, **1967**, 6, 2262.

(25) Song, K. University of Iowa, unpublished result.

(26) Gloer, K. B. University of Iowa, unpublished result.

(27) LaBrush, D. M. University of Iowa, unpublished result.

(28) Beamish, F. E. *The Analytical Chemistry of the Nobel Metals*, Pregamon, New York, 1966.

(29) Gay, I. D. *J. Catal.*, **1983**, 231.

(30) Wu, X. Ph. D. Thesis, Iowa State University, 1990.

(31) Marczenko, *Separation and Spectroscopic Determination of the Elements*; Halsted; New York, 1986; p 493.

(32) a) Howe, J. L. *J. Am. Chem. Soc.*, **1901**, 23, 777.
b) Brauer, G. *Handbook of Preparative Inorganic Chemistry; Vol. II*, Academic, New York, 1965.
c) Jacobson, C. A., Encyclopedia of Chemical Reactions; Vol V, Renhold, New York, 1959.

(33) Perrin, D. D. and Armarego, W. L. F.; *Purification of Laboratory Chemicals*; Pergamon, New York, 1988.

(34) Anderson, J. R. *Structure of Metallic Catalysts*; Academic; New York; 1975.

(35) a) Narita, T., Miura, H., Sugiyama, T., Matsuda, T., and Gonzalex, R., J. Catal., **1987**, 103, 492-495.
b) Narita, T., Miura, H., Sugiyama, T., Matsuda, T., and Gonzalex, R. *J. Catal.*, **1987**, 103, 185–190.

(36) a) Lu, K., Tatarchuk, B. *J. Catal.* **1987**, 106, 166.
b) Lu, K., Tatarchuk, B. *J. Catal.* **1987**, 106, 175.

(37) Miura, H., Hondou, H., Sugiyama, T., Matsuda, T., and Gonzalex, R., J. International Congress on Catalysis Proceedings; Amsterdam

(38) Fubara, B., Accel Catalysis, Inc., Unpublished Results.

(39) Wang, W., University of Iowa, Unpublished Results.

(40) Somorjai, G. *Chemistry in Two Dimensions: Surfaces*; Cornell University; Ithaca; 1981.

(41) Dalla Betta, R. A. *J. Catal.*, **1974**, 34, 57.

(42) a) Goodwin, J. *J. Catal.* **1981**,68, 227.
b) Yang, C., Goodwin, J. G. *J. Catal.* **1982**, 78, 182.

(43) a) Clausen, C. A., Good, M. L. *J. Catal*, **1975**, 38, 92.
b) King, D. L. *J. Catal.*, **1978**, 51, 386.
c) Koopman, D. L., Kieboom, A. P., Van Bekkum, H. *J. Catal.*, **1981**, 69, 172.